[American Journal of Science, Vol. 314, February, 2014, P. 580–612, DOI 10.2475/02.2014.05]

ZIRCON U-Pb GEOCHRONOLOGY AND Hf ISOTOPIC COMPOSITION OF GRANITIODS IN RUSSIAN ALTAI MOUNTAIN, CENTRAL ASIAN OROGENIC BELT

KEDA CAI*,**, MIN SUN**,†, WENJIAO XIAO*,***, M. M. BUSLOV§, CHAO YUAN§§, GUOCHUN ZHAO**, and XIAOPING LONG*

ABSTRACT. The Central Asian Orogenic Belt (CAOB) consists of many tectonic terranes with distinct origin and complicated evolutionary history. Understanding of individual block is crucial for the reconstruction of the geodynamic history of the gigantic accetionary collage. This study presents zircon U-Pb ages and Hf isotopes for the granitoid rocks in the Russian Altai mountain range (including Gorny Altai, Altai-Mongolian terrane and CTUS suture zone between them), in order to clarify the timing of granitic magmatism, source nature, continental crustal growth and tectonic evolution.

Our dating results suggest that granitic magmatism of the Russian Altai mountain range occurred in three major episodes including 445~429 Ma, 410~360 Ma and ~241 Ma. Zircons from these granitoids yield comparable positive $\varepsilon_{Hf}(t)$ values and Neoproterozoic crustal model ages, which favor the interpretation that the juvenile crustal materials produced in the early stage of the CAOB were probably dominant sources for the Paleozoic magmatism in the region. The inference is also supported by widespread occurrence of short-lived juvenile materials including ophiolites, seamount relics and arc assemblages in the northern CAOB. Consequently, the Paleozoic massive granitic rocks maybe do not represent continental crustal growth at the time when they were emplaced, but rather record reworking of relatively juvenile Proterozoic crustal rocks although mantle-derived mafic magma was possibly involved to serve as heat engine during granitic magma generation. The Early Triassic granitic intrusion may be a product in an intra-plate environment, as the case of same type rocks in the adjacent areas. The positive $\varepsilon_{Hf}(t)$ values (1.81~7.47) and corresponding Hf model ages (0.80~1.16 Ga) together with evidence of petrology are consistent with the interpretation that the magma source of the Triassic granitic intrusion was derived from enriched mantle and melted under an usually high temperature condition likely due to basaltic magma that underplated the lower crust.

Our data combined with evidence of the regional geology enable us to conclude that the Gorny Altai and Altai-Mongolian terranes possibly have similar tectonic natures, but represent two separate accretionary systems before Devonian collision. The accretion and amalgamation processes resulted in the Paleozoic granitoid magmatism and caused the two terranes to merge as a composite tectonic domain at the Siberian continental margin.

Key words: Central Asian Orogenic Belt, Gorny Altai, Altai-Mongolian terrane, zircon U-Pb age, Hf isotope, Paleozoic tectonic evolution

* Xinjiang Research Center for Mineral Resources, Xinjiang Institute of Ecology and Geography, Chinese Academy of Sciences, Urumqi 830011, China

** Department of Earth Sciences, The University of Hong Kong, Pokfulam Road, Hong Kong, China

*** State Key Laboratory of Lithospheric Evolution, Institute of Geology and Geophysics, Chinese Academy of Sciences, Beijing 100029, China

§ Institute of Geology and Mineralogy, Siberian Branch of the RAS, 3 prosp. Akad. Koptyuga, 630090 Novosibirsk, Russia

§§ Key Laboratory of Isotope Geochronology and Geochemistry, Guangzhou Institute of Geochemistry, Chinese Academy of Sciences, Guangzhou 510640, China

† Corresponding author: E-mail: minsun@hku.hk; Tel: (852) 28592194 or 62746604; Fax: (852) 25176912

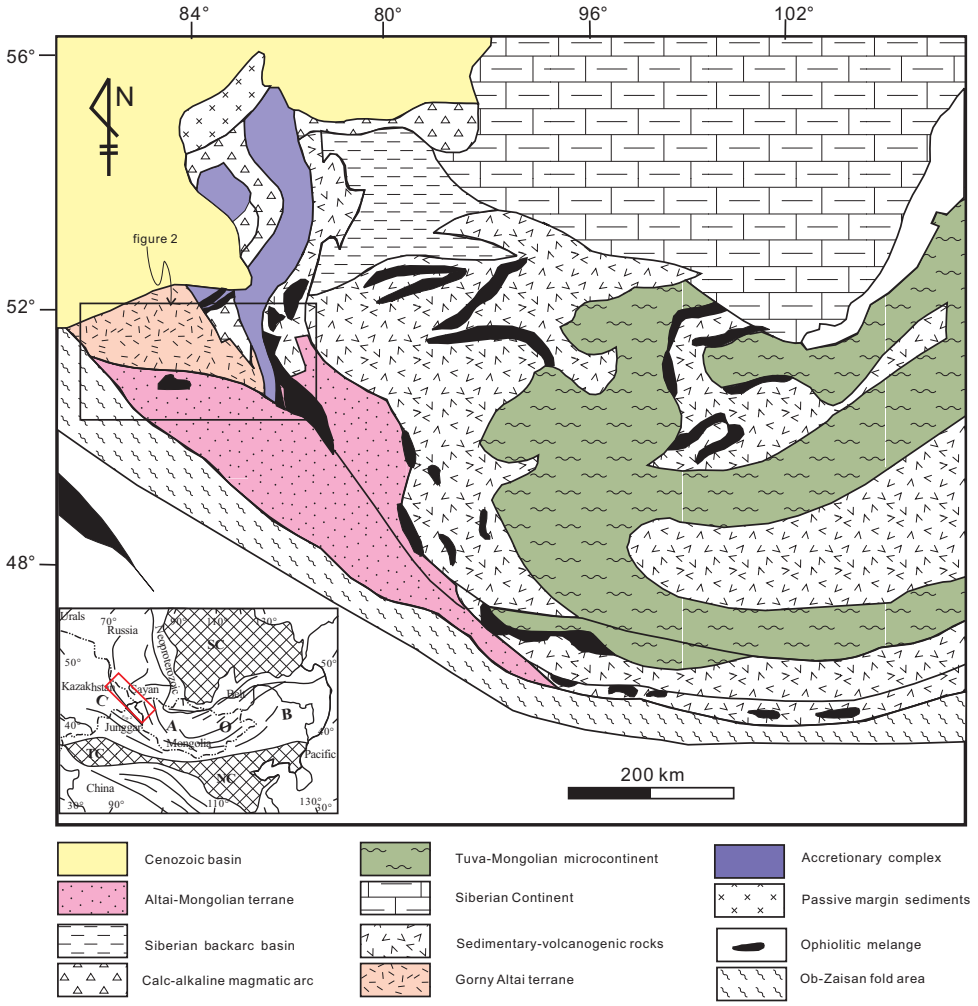

Fig. 1. Simplified geological map and tectonic units of the Russian Altai mountain range and its surrounding areas (after Dobretsov and Buslov, 2007; Buslov and Safonova, 2010; Glorie and others, 2011). Inset figure shows location of the CAOB. The Russian Altai mountain range is indicated by a black box. SC–Siberian Craton, TC–Tarim Craton, NC–North China Craton.

INTRODUCTION

The Central Asian Orogenic Belt (CAOB), also named as the Altaids, is one of the largest accretionary orogenic belts in the world (Sengör and others, 1993; Mossakovsky and others, 1993; Sengör and Natal'in, 1996; Jahn and others, 2000a, 2000b; Kovalenko and others, 2004; Windley and others, 2007; Wilhem and others, 2012). It encompasses an immense area that extends from the Urals in the west to the Pacific coast in the east and from the Siberian Craton in the north to the North China and Tarim Cratons in the south (fig. 1, inset). The architecture of CAOB is generally attributed to progressive accretion of numerous island arcs, paleo-seamounts, oceanic plateaus, ophiolites and micro-continents (fig. 1, Khain and others, 2002; Yakubchuk, 2004; Jahn and others, 2004; Xiao and others, 2004, 2008, 2009, 2010; Kuzmichev and others, 2005; Windley and others, 2007).

However, it is difficult to reveal tectonic affinity of each individual block in the huge accretionary orogenic belt because of its long-lived subduction-accretion and amalgamation history. Controversies exist on the tectonic nature of many blocks, which seriously retard our understanding of the accretionary orogenesis and mechanism of crustal growth. For instance, the Altai-Mongolian Terrane was regarded as a microcontinent (Windley and others, 2002; Li and others, 2006; Wang and others, 2009), a subduction-accretion complex (Long and others, 2010; Cai and others, 2011c), or an active continental margin (Sun and others, 2008; Liu and others, 2012). The Russian Altai mountain range, located to the north of the Chinese Altai, occupies a critical position in the CAOB (fig. 1), which represent a junction among the Siberian active margin, the composite Kazakhstan continent and the Altai-Mongolian Terrane. However, little constraint has been imposed on tectonic nature and evolution of this key area, although several tectonic units are roughly identified (Gorny Altai, Berzin and Dobretsov, 1994; Buslov and others, 2001; Altai-Mongolian Terrane, Windley and others, 2007; Charysh-Terekta-Ulagan-Sayan suture-shear zone, Buslov and others, 2004a; Glorie and others, 2011).

One of the most distinctive characteristics of the Russian Altai mountain range is the wide distribution of voluminous granitic intrusions. Available data documented that these granitic plutons intruded in a long time interval from the Paleozoic to the Mesozoic, and most of them have I-type or A-type affinities (Kruk and others, 2011; Glorie and others, 2011). Detailed study is lacking, although in general, the I-type granites are regarded to be petrogenetically linked to the subduction of the Paleoasian Ocean (Wang and others, 2006; Yuan and others, 2007; Tong and others, 2007; Sun and others, 2008; Cai and others, 2011a, 2011b), whereas, A-type granites are considered to be associated with post-collision extension (Han and others, 1997; Jahn and others, 2009; Reichow and others, 2010; Tsygankov and others, 2010; Litvinovsky and others, 2011).

In the current contribution, representative granites were collected from the Russian Altai mountain range (figs. 2 and 3), and systematic zircon U-Pb geochronological and Lu-Hf isotopic studies were carried out. Our data place firm constraints on timing of emplacement and source nature of the granitic magmas, which enable us to further discuss the mechanism of crustal growth and tectonic evolution of the CAOB.

GEOLOGICAL BACKGROUND

The Altai mountain range is located in the central area of the CAOB and stretches about 2500 km from the Siberian Cenozoic basin in the west to the northern border of the North China Craton in the east (fig. 1). It is composed of several mountain domains in Russia, Mongolia, China, and Kazakhstan. The term Russian Altai is used here for variable tectonic units in the Altai mountain section in Russia, specifically, including the Gorny Altai terrane, part of the Altai-Mongolian terrane and Charysh-Terekta-Ulagan-Sayan suture-shear zone (CTUSs) (fig. 2; Dobretsov and Buslov, 2007; Buslov, 2011).

The Gorny Altai is a triangle-shaped tectonic unit situated in the northwestern CAOB, separated by the Charysh-Terekta-Ulagan-Sayan suture-shear zone (CTUSs) from the Altai-Mongolian terrane in the south and West-Sayan Paleo-island arc belt in the east (figs. 1 and 2). The early evolution of the Gorny Altai is attributed to an intra-oceanic subduction system in the Early Ediacaran-Early Cambrian, as a result of transition from a transform fault zone into an incipient subduction zone close to the Siberian margin (Ota and others, 2007; Glorie and others, 2011). Well-preserved Late Neoproterozoic to Early Cambrian subduction-accretion complexes in the Gorny Altai may represent the early stage of the tectonic evolution of the immense CAOB (fig. 1; Buslov and others, 1993, 1998, 2001; Buslov and Watanabe, 1996). Subduction-accretion complexes with ages of Late Neoproterozoic to Early Cambrian include the

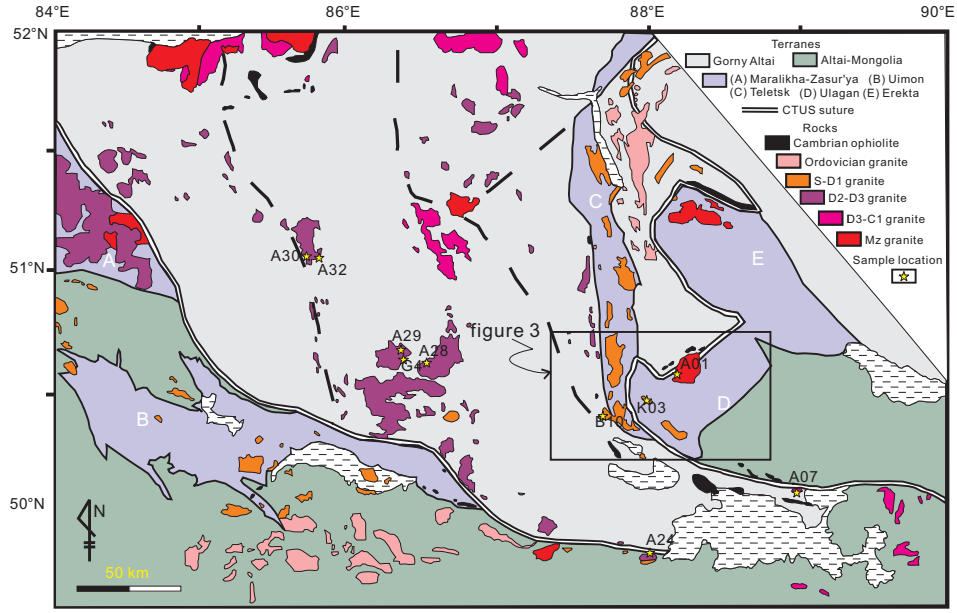

Fig. 2. Schematic geological map of the Charysh-Terekta-Ulagan-Sayan suture zone (CTUSs) and the neighbouring Gorny Altai and Altai-Mongolian terranes (from Glorie and others, 2011).

Kuznetsk-Altay island arc system, accretionary prisms (including paleo-seamount), ophiolite and eclogite-bearing high-pressure metamorphic belt. In the Late Cambrian-Early Ordovician, island arc blocks and other accretionary complexes accreted to the south margin of the Siberian Craton and an orogenic belt was formed (Berzin and Dobretsov, 1994; Buslov and others, 2001; Dobretsov and others, 2003). The Gorny Altai was under a passive margin regime in the Ordovician–Silurian when up to 4.5 to 6 km thick submarine terrigeneous-carbonate sediments were extensively accumulated in a shallow-water shelf setting (Kruk and others, 2011 and reference therein). In the Devonian, the geodynamic environment of the Gorny Altai changed into an active continental margin, which is documented by a suite of volcanic rocks including rhyolite-dacitic lava and tuffs. In the Middle-Late Devonian, collision between the Gorny Altai and the Altai-Mongolian terrane caused deformation of sedimentary basins and blueschist-grade metamorphism (Volkova and others, 2005; Volkova and Skllarov, 2007), high temperature and low pressure metamorphism, and basaltic and granitic magmatism (Vladimirov and others, 2001; Rudnev and others, 2004, 2008).

The Altai-Mongolian terrane is separated by faults and strike-slip zone from surrounding terranes, and is situated to the southeast of the Gorny Altai and covers a vast area of 1000 km long and up to 500 km wide (figs. 1 and 2). This terrane was considered as a Gondwana-derived micro-continent (Zonenshain and others, 1990; Mossakovsky and others, 1993; Ruzhentsev and Mossakovskiy, 1996; Dobretsov and others, 2003; Buslov and others, 2004a, 2004b; Dobretsov and Buslov, 2007; Glorie and others, 2011; Yang and others, 2011), but no solid evidence for the existence of Precambrian basement rocks. Precambrian ages are limited to some detrital zircons from metasedimentary rocks and inherited zircons from granitoids (Long and others, 2007, 2010; Sun and others, 2008, 2009; Jiang and others, 2011; Cai and others, 2011a; Glorie and others, 2011). The Altai-Mongolian terrane is apparently characterized by immensely thick sedimentary succession of rhythmically bedded quartzo-feldspar

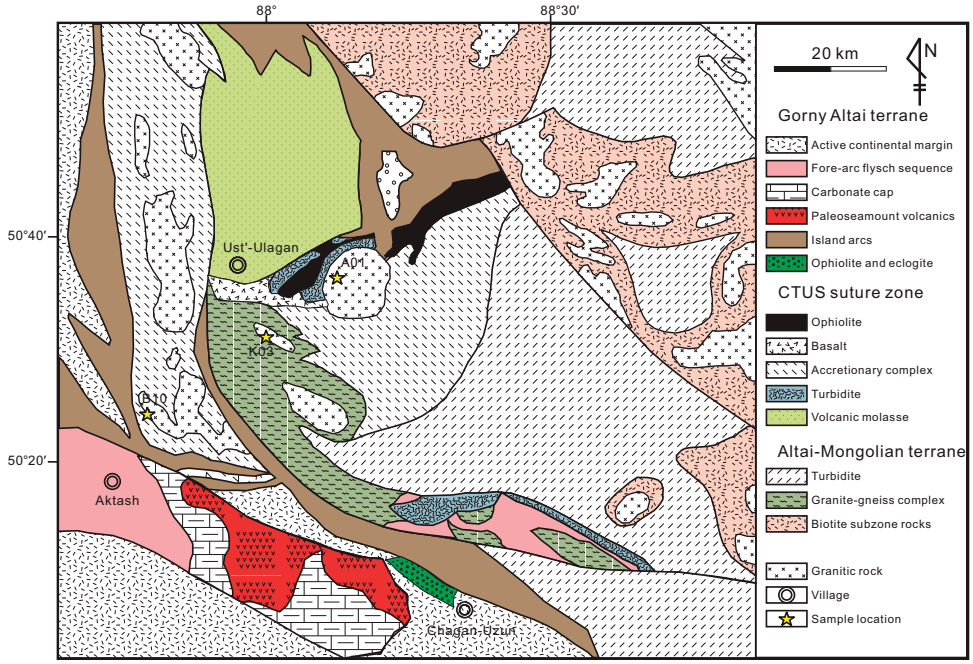

Fig. 3. Simplified geological map and tectonic units of the region between the Gorny Altai and the Altai-Mongolian terrane (from Buslov and Safonova, 2010).

sediments including sandstones, siliceous and phyllitic shales (Buslov and Safonova, 2010). The rhythmic flysch sequences are folded and progressively overlain by Ordovician-Devonian gray marine sediments that are in turn, covered by Devonian volcanic rocks. A larger number of granitoid plutons intruded into these sedimentary rocks (figs. 2 and 3).

The Charysh-Terekta-Ulagan-Sayan suture-shear zone (CTUSs) is EW-striking and divided by transverse strike-slip faults into several segments (fig. 2). The suture zone contains abundant ophiolites, remnants of island arc, turbiditic rocks and high pressure metamorphic rocks (fig. 3; Buslov and others, 2004a, 2004b; Volkova and others, 2005; Volkova and Sklyarov, 2007). According to the previous perception that the Altai-Mongolian terrane is an important portion of the Kazakhstan-Baikal composite continent originally associated with the Gondwana supercontinent and differs essentially from the Gorny Altai of the Siberian continental periphery, the CTUSs is regarded as the final tectonic boundary between the two tectonic realms.

ANALYTICAL METHODS

Zircon Separation and CL Imaging

After sample crushing, zircons were separated by standard heavy liquid and magnetic techniques. Crystal grains from the >25 μm non-magnetic fractions were hand-picked and mounted on adhesive tape, then enclosed in epoxy resin and polished to about half of their thickness. Cathodoluminescence (CL) images were obtained using a JXA-8100 Electron Probe Micro-analyzer with a Mono CL3 Cathodoluminescence System for high resolution imaging and spectroscopy at Guangzhou Institute of Geochemistry, Chinese Academy of Sciences, in order to investigate internal structures and choose potential target sites for U-Pb and Hf analyses.

Zircon U-Pb Isotopic Analyses

Zircon U-Pb dating was preformed at the Department of Earth Sciences, the University of Hong Kong. A 193 nm excimer laser ablation system (Resolution M-50) was used in connection with a Nu Plasma HR MC-ICP-MS. The detailed analytical procedure was described by Xia and others (2011). Most analyses were conducted with a beam diameter of 40 μm, 5 Hz repetition rate and energy of ~5 J/cm^2 per pulse. Zircon standard 91500 and GJ-1 were used as the external standard for calibration. The mass fractionation correction and isotopic results were calculated by ICPMSDataCal (version 7.0, Liu and others, 2008). A common Pb correction was applied to all measured ratios using the interference and background-corrected ^{204}Pb signal intensity following the model of Andersen (2002). The age calculation and concordia plots were processed using ISOPLOT (version 3.0, Ludwig, 2003). Individual analyses are presented with 1σ error, and uncertainties in mean age calculations are quoted at the 95 percent level (2σ). ^{206}Pb/^{238}U ages are used for grains <1.0 Ga, and ^{207}Pb/^{206}Pb ages are used for grains >1.0 Ga, suggested by Black and others (2003).

Zircon Hf Isotopic Analyses

Zircon Hf isotopic analyses was also carried out using the laser ablation system Resolution M-50, attached to a Nu Plasma HR MC-ICPMS, at the University of Hong Kong. A spot size of 40 μm was used for most analyses and the ablation spot for Hf analysis was sited at the same and/or near domain for the U-Pb dating. In the case of isotopic zoning or with intersecting cracks/inclusions, only the flattest and most stable portions of the time-resolved signal were selected for integration. Zircon standards 91500 and GJ-1 were used as reference materials. Detailed instrumental settings and analytical procedures were described by Xia and others (2011). All Hf isotope data were calculated using the decay constant of 1.865×10^{-11} yr^{-1} as reported by Schärer and others (2001). The chondritic values of ^{176}Hf/^{177}Hf = 0.0332 and ^{176}Lu/^{177}Hf = 0.282772 reported by Blichert-Toft and others (1997) were used for the calculation of $\varepsilon_{Hf}(t)$ values. The depleted mantle evolution line is defined by present-day ^{176}Hf/^{177}Hf = 0.28325 and ^{176}Lu/^{177}Hf = 0.0384 (Griffin and others, 2004). Because most of the granites are partial melts of crustal rocks although few are mantle-derived via extensive fractional crystallization, a two-stage model age (T^C_{DM}) is more meaningful than a depleted mantle model age (Griffin and others, 2004; Belousova and others, 2006). However, for the granites in the CAOB, they are considered to be derived from juvenile crustal sources, in this study, therefore, both the two-stage model age (T^C_{DM}) and the depleted mantle model age (T_{DM}) were calculated for comparison, assuming mean^{176}Lu/^{177}Hf ratio of 0.015 for the bulk continental crust (Griffin and others, 2004).

ANALYTICAL RESULTS

Ten granitic samples were systemically collected from the Russian Altai Mountain and sample descriptions including locality and mineral assemblage are summarized in table 1. Analytical results of zircon U-Pb age and Hf isotope are presented in tables 2 and 3, respectively.

Granitic Samples of the Gorny Altai Terrane

Kurata granite-leucogranite intrusions were emplaced into an accretionary complex at the Devonian active margin of the Gorny Altai terrane. The complex consists chiefly of the Kurata formation, which consists mainly of volcanic rocks with more felsic composition upwards. The magmatic rocks include rhyolite-dacite porphyries and granite-leucogranite intrusions. In this study, representative samples of granite (sample A30) and leucogranite (sample A32) were collected for zircon U-Pb dating and Hf isotopic analyses. Zircon CL images of the two samples exhibit euhedral and prismatic

TABLE 1

Description of granitoid samples from the Russian Altai

Sample	Latitude	Longitude	Locality	Lithology	Grain size	Mineral assemblage
A30	51°05'54.2"N	85°35'8.7"E	Gorny Altai	Granite	Medium	Qz+Kf+Pl+Bi+Zr
A32	51°05'54.2"N	85°35'8.7"E	Gorny Altai	Leucogranite	Fine	Qz+Kf+Pl+Ms+Zr
G4	50°38'45.2"N	86°18'44.8"E	Gorny Altai	Granodiorite	Medium	Qz+Pl+Hbl+Bi+Zr+Mgn
A29	50°38'42.8"N	86°18'43.1"E	Gorny Altai	Tonalite	Medium	Qz+Pl+Hbl+Bi+Zr+Mgn
A28	50°37'49.1"N	86°25'03.2"E	Gorny Altai	Gneissic granite	Medium	Qz+Kf+Pl+Bi+Zr
A07	50°06'18.1"N	88°53'26.5"E	Altai-Mongolian	Granite	Medium	Qz+Kf+Pl+Bi+Hbl+Zr
K03	50°14'32"N	87°58'49.2"E	Altai-Mongolian	Granodiorite	Coarse	Qz+Pl+Kf+Hbl+Bi+Zr+Mgn
B10	50°26'42.7"N	87°36'23.3"E	CTUS	Gneissic granite	Medium	Qz+Kf+Pl+Bi+Hbl+Zr
A24	49°57'45.4"N	88°04'30.2"E	CTUS	Granodiorite	Medium	Qz+Pl+Hbl+Bi+Zr+Mgn
A01	50°32'02.3"N	88°10'32.0"E	CTUS	Two-mica granite	Coarse	Qz+Kf+Pl+Bi+Ms+Zr

Qz=Quartz, Pl=plagioclase, Kf=K-feldspar, Bt= biotite, Hbl=Hornblende, Ms=muscovite, Zr=Zircon, Mgn=Magnetite, Sil=Sillmantite, Grt=Garnet, Chl=Chlorite.

shape, with oscillatory zoning and without inherited cores (fig. 4). These features and high Th/U ratios (>0.1) indicate an igneous origin (Hoskin and Schaltegger, 2003).

Sample A30: Nine zircon spots were analyzed for U-Pb isotopic compositions, which give $^{206}Pb/^{238}U$ ages ranging from 344 to 401 Ma, and an upper intercept age of 401 Ma (fig. 5A). The $\varepsilon_{Hf}(t)$ values of these zircons are from +7.8 to +11.3, and corresponding T^{C}_{DM} model ages are from 0.68 to 0.90 Ga (table 3 and fig. 6A).

Sample A32: Ten zircon analyses cluster between 407 and 400 Ma, giving a weighted mean $^{206}Pb/^{238}U$ age of 401 ±2 Ma (fig. 5B). The $\varepsilon_{Hf}(t)$ values of these zircons are from +7.85 to +12.1, and corresponding T^{C}_{DM} model ages are from 0.63 to 0.90 Ga (table 3 and fig. 6B).

Chiketaman batholith is located around the Chiketaman pass of the Gorny Altai terrane (fig. 2). With an outcrop area of 80 km^2, this batholith consists mainly of tonalite, quartz diorite and granodiorite. In this study, one granodiorite (sample G4) and one tonalite (sample A29) were collected for zircon U-Pb dating and Hf isotopic analyses. Zircons from the two samples are characterized by euhedral and prismatic shape, with oscillatory zoning and without inherited cores (fig. 4). All analyzed zircons have high Th/U ratios (>0.1), implying an igneous origin (Hoskin and Schaltegger, 2003).

Sample G4: Sixteen analyzed zircon spots cluster between 347 and 372 Ma and yield a weighted mean $^{206}Pb/^{238}U$ age of 360 ±5 Ma (fig. 5D). These zircons yielded variable Hf isotopic compositions with $\varepsilon_{Hf}(t)$ values ranging from −2.1 to +11.3, and their T^{C}_{DM} model ages vary from 0.65 to 1.51 Ga (table 3 and fig. 6D).

Sample A29: Fourteen zircon spots were analyzed for U-Pb isotopic compositions and yielded $^{206}Pb/^{238}U$ ages ranging from 367 to 413 Ma, with a weighted mean $^{206}Pb/^{238}U$ age of 384 ±7 Ma (fig. 5C). The $\varepsilon_{Hf}(t)$ values of these zircons fall in a broad range from −3.5 to +10.1, and corresponding T^{C}_{DM} model ages are from 0.74 to 1.61 Ga (table 3 and fig. 6C).

Kadrin batholith is situated to the east of the Chiketaman batholith along the main road of the Gorny Altai terrane. The batholith, similar to the Chiketaman batholith, intruded into an assumed Early Paleozoic passive margin with a thick sequence of conglomerate, sandstone, mudstone and limestone. The outcrop area of the batholith is about 100 km^2, and it consists mainly of granite and alaskite. One deformed granitic rock was sampled for zircon U-Pb dating and Hf isotopic analyses.

Sample A28: All zircons separated from this sample display euhedral and prismatic shape, with oscillatory zoning (fig. 4), and have high Th/U ratios (>0.1), suggestive of magmatic origin (Hoskin and Schaltegger, 2003). Twelve zircons were

TABLE 2

LA-ICPMS U-Pb isotopic data for zircons from granitoids in the Russian Altai

Sample	Ratios							Ages (Ma)						
Spot No.	Th/U	$^{207}Pb/^{206}Pb$	1σ	$^{207}Pb/^{235}U$	1σ	$^{206}Pb/^{238}U$	1σ	$^{207}Pb/^{206}Pb$	1σ	$^{207}Pb/^{235}U$	1σ	$^{206}Pb/^{238}U$	1σ	Disc. (%)
A30 (51°05'54.2"N, 85°35'8.7"E)														
1	0.23	0.05557	0.00236	0.49070	0.02190	0.06406	0.00209	435	24	405	16	400	18	1
2	0.43	0.05520	0.00301	0.48814	0.02644	0.06409	0.00209	420	23	404	16	400	18	1
3	0.40	0.05507	0.00235	0.48720	0.02181	0.06411	0.00210	415	20	403	14	401	16	0
4	0.58	0.05669	0.00262	0.46425	0.02097	0.05941	0.00184	479	17	387	10	372	12	4
5	0.25	0.05872	0.00247	0.44266	0.02141	0.05476	0.00199	557	12	372	8	344	8	8
6	0.12	0.05528	0.00370	0.44535	0.03143	0.05839	0.00223	423	9	374	6	366	6	2
7	0.24	0.05583	0.00272	0.49379	0.02260	0.06416	0.00201	446	8	407	6	401	6	1
8	0.36	0.05469	0.00281	0.48164	0.02307	0.06391	0.00204	400	14	399	8	399	8	0
9	0.21	0.05861	0.00283	0.45236	0.02430	0.05614	0.00215	553	15	379	10	352	8	7
A32 (51°05'54.2"N, 85°35'8.7"E)														
1	0.23	0.05514	0.00042	0.49253	0.00656	0.06487	0.00081	418	13	407	4	405	5	0
2	0.27	0.05511	0.00040	0.49464	0.00588	0.06522	0.00070	417	12	408	4	407	4	0
3	0.25	0.05536	0.00037	0.48976	0.00524	0.06417	0.00053	427	11	405	4	401	3	1
4	0.14	0.05558	0.00049	0.49226	0.00683	0.06411	0.00058	436	16	406	5	401	4	1
5	0.04	0.05520	0.00066	0.48751	0.00740	0.06402	0.00058	420	19	403	5	400	3	1
6	0.13	0.05479	0.00043	0.48442	0.00505	0.06416	0.00047	404	11	401	3	401	3	0
7	0.12	0.05411	0.00050	0.47943	0.00566	0.06429	0.00051	376	13	398	4	402	3	-1
8	0.34	0.05499	0.00041	0.48652	0.00630	0.06406	0.00060	412	14	403	4	400	4	1
9	0.36	0.05495	0.00039	0.48494	0.00522	0.06401	0.00053	410	11	401	4	400	3	0
10	0.21	0.05623	0.00049	0.49563	0.00542	0.06406	0.00047	462	12	409	4	400	3	2
G4 (50°38'45.2"N, 86°18'44.8"E)														
1	0.25	0.06270	0.00156	0.47849	0.02017	0.05535	0.00175	698	54	397	32	347	12	13
2	0.14	0.05693	0.00034	0.44639	0.02190	0.05693	0.00209	489	9	375	12	357	12	5
3	0.13	0.05550	0.00027	0.42627	0.02181	0.05565	0.00210	432	10	361	12	349	8	3
4	0.12	0.05486	0.00022	0.44093	0.02097	0.05830	0.00184	406	7	371	8	365	8	2
5	0.25	0.06153	0.00056	0.48878	0.02141	0.05794	0.00199	658	9	404	12	363	12	10
6	0.14	0.05512	0.00041	0.44491	0.02217	0.05868	0.00197	417	9	374	12	368	12	2

TABLE 2
(continued)

Sample	Ratios							Ages (Ma)						
Spot No.	$\frac{Th}{U}$	$\frac{^{207}Pb}{^{206}Pb}$	1σ	$\frac{^{207}Pb}{^{235}U}$	1σ	$\frac{^{206}Pb}{^{238}U}$	1σ	$\frac{^{207}Pb}{^{206}Pb}$	1σ	$\frac{^{207}Pb}{^{235}U}$	1σ	$\frac{^{206}Pb}{^{238}U}$	1σ	Disc. (%)
G4 (50°38'45.2"N, 86°18'44.8"E)														
7	0.04	0.05570	0.00051	0.44058	0.02772	0.05736	0.00272	440	14	371	16	360	12	3
8	0.13	0.05453	0.00035	0.44583	0.01887	0.05932	0.00200	393	11	374	12	372	12	1
9	0.12	0.05524	0.00047	0.44262	0.01924	0.05819	0.00181	422	12	372	16	365	12	2
10	0.34	0.05676	0.00035	0.43816	0.03143	0.05592	0.00223	482	9	369	12	351	8	5
11	0.36	0.05705	0.00041	0.46068	0.02571	0.05847	0.00202	493	13	385	16	366	12	5
12	0.21	0.05550	0.00039	0.44836	0.02260	0.05856	0.00201	432	11	376	12	367	8	2
13	0.40	0.06129	0.00060	0.47980	0.02325	0.05696	0.00155	650	9	398	12	357	12	10
14	0.58	0.05510	0.00046	0.44710	0.02307	0.05882	0.00204	416	13	375	16	368	12	2
15	0.25	0.06095	0.00055	0.46868	0.02595	0.05591	0.00216	637	11	390	16	351	12	10
16	0.12	0.05522	0.00058	0.43929	0.02430	0.05749	0.00215	421	16	370	20	360	16	3
A29 (50°38'42.8"N, 86°18'43.1"E)														
1	0.33	0.05949	0.00263	0.47992	0.02017	0.05863	0.00175	585	12	398	12	367	12	8
2	0.23	0.05906	0.00236	0.49067	0.02190	0.06021	0.00209	569	11	405	12	377	12	7
3	0.43	0.05935	0.00301	0.48887	0.02644	0.05982	0.00209	580	15	404	12	375	12	7
4	0.40	0.05810	0.00235	0.47947	0.02181	0.05983	0.00210	533	10	398	9	375	12	6
5	0.58	0.06022	0.00262	0.53440	0.02097	0.06433	0.00184	612	11	435	12	402	16	8
6	0.27	0.05555	0.00234	0.46726	0.02106	0.06107	0.00205	434	10	389	9	382	12	2
7	0.12	0.05585	0.00203	0.47116	0.01744	0.06119	0.00192	446	13	392	12	383	12	2
8	0.25	0.05505	0.00247	0.48144	0.02141	0.06340	0.00199	414	15	399	12	396	16	1
9	0.14	0.05495	0.00265	0.48081	0.02217	0.06345	0.00197	410	13	399	12	397	12	1
10	0.04	0.05856	0.00235	0.50808	0.02772	0.06298	0.00272	551	12	417	12	394	12	6
11	0.37	0.05618	0.00248	0.46177	0.01924	0.05957	0.00181	459	20	385	15	373	12	3
12	0.12	0.06188	0.00370	0.50773	0.03143	0.05941	0.00223	670	20	417	18	372	16	11
13	0.65	0.05565	0.00398	0.50764	0.02325	0.06612	0.00155	438	11	417	12	413	16	1
14	0.29	0.05481	0.00302	0.47953	0.02595	0.06343	0.00216	405	9	398	9	396	12	1

Table 2
(continued)

Sample	Ratios							Ages (Ma)						
Spot No.	Th/U	$^{207}Pb/^{206}Pb$	1σ	$^{207}Pb/^{235}U$	1σ	$^{206}Pb/^{238}U$	1σ	$^{207}Pb/^{206}Pb$	1σ	$^{207}Pb/^{235}U$	1σ	$^{206}Pb/^{238}U$	1σ	Disc. (%)
A28 (50°37'49.1"N, 86°25'03.2"E)														
1	0.23	0.05651	0.00236	0.41004	0.02190	0.05246	0.00209	473	19	349	5	330	4	5
2	0.43	0.05547	0.00301	0.46902	0.02644	0.06126	0.00209	431	15	391	4	383	3	2
3	0.40	0.05507	0.00235	0.42815	0.02181	0.05634	0.00210	415	12	362	4	353	3	2
4	0.25	0.05808	0.00247	0.38639	0.02141	0.04820	0.00199	533	12	332	4	303	3	9
5	0.14	0.05895	0.00265	0.36563	0.02217	0.04493	0.00197	565	18	316	5	283	3	10
6	0.04	0.05550	0.00235	0.39645	0.02772	0.05174	0.00272	432	12	339	3	325	3	4
7	0.37	0.05528	0.00248	0.40844	0.01924	0.05361	0.00181	424	13	348	4	337	3	3
8	0.12	0.05993	0.00370	0.37362	0.03143	0.04519	0.00223	601	11	322	3	285	2	11
9	0.34	0.05724	0.00315	0.38342	0.02571	0.04854	0.00202	501	16	330	4	306	2	7
10	0.24	0.05638	0.00272	0.45961	0.02260	0.05912	0.00201	467	10	384	3	370	3	4
11	0.65	0.05502	0.00398	0.47303	0.02325	0.06235	0.00155	413	15	393	5	390	5	1
12	0.21	0.05589	0.00283	0.42542	0.02430	0.05524	0.00215	448	14	360	4	347	3	4
A07 (50°06'18.1"N, 88°53'26.5"E)														
1	0.33	0.05508	0.00038	0.50495	0.00665	0.06642	0.00072	416	13	415	4	415	4	0
2	0.40	0.05583	0.00026	0.51114	0.00507	0.06640	0.00058	446	10	419	3	414	3	1
3	0.58	0.05600	0.00039	0.51133	0.00612	0.06634	0.00073	453	12	419	4	414	4	1
4	0.27	0.05496	0.00036	0.49550	0.00486	0.06535	0.00045	411	11	409	3	408	3	0
5	0.34	0.05669	0.00031	0.50162	0.00425	0.06424	0.00046	479	8	413	3	401	3	3
6	0.25	0.05594	0.00049	0.51608	0.00672	0.06712	0.00082	450	13	423	4	419	5	1
7	0.04	0.05600	0.00044	0.50439	0.00670	0.06527	0.00068	452	14	415	5	408	4	2
8	0.13	0.05611	0.00032	0.50781	0.00518	0.06572	0.00059	457	10	417	3	410	4	2
9	0.37	0.05530	0.00032	0.50290	0.00727	0.06589	0.00086	424	14	414	5	411	5	1
10	0.12	0.05523	0.00029	0.49389	0.00535	0.06488	0.00065	422	11	408	4	405	4	1
11	0.24	0.05478	0.00056	0.48791	0.01171	0.06452	0.00152	403	24	403	8	403	9	0
12	0.65	0.05508	0.00028	0.49878	0.00641	0.06564	0.00079	415	13	411	4	410	5	0
13	0.29	0.05643	0.00035	0.51108	0.00704	0.06573	0.00086	469	14	419	5	410	5	2
14	0.21	0.05578	0.00046	0.51264	0.00876	0.06674	0.00105	443	17	420	6	416	6	1

TABLE 2
(continued)

Sample	Ratios							Ages (Ma)						
Spot No.	Th/U	$^{207}Pb/^{206}Pb$	1σ	$^{207}Pb/^{235}U$	1σ	$^{206}Pb/^{238}U$	1σ	$^{207}Pb/^{206}Pb$	1σ	$^{207}Pb/^{235}U$	1σ	$^{206}Pb/^{238}U$	1σ	Disc. (%)
K03 (50°14'32"N, 87°58'49.2"E)														
1	0.33	0.05672	0.00083	0.48247	0.00772	0.06169	0.00047	481	19	400	5	386	3	4
2	0.23	0.05742	0.00058	0.50138	0.00589	0.06334	0.00047	508	10	413	4	396	3	4
3	0.12	0.05566	0.00069	0.50766	0.00823	0.06614	0.00071	439	13	417	6	413	4	1
4	0.34	0.05558	0.00030	0.48156	0.00429	0.06282	0.00046	436	4	399	3	393	3	2
5	0.25	0.05450	0.00052	0.46748	0.00606	0.06219	0.00053	392	10	389	4	389	3	0
6	0.14	0.05467	0.00051	0.48075	0.01556	0.06438	0.00228	399	7	399	11	402	14	-1
7	0.04	0.05459	0.00050	0.47100	0.00601	0.06254	0.00054	395	10	392	4	391	3	0
8	0.34	0.05460	0.00042	0.47114	0.00489	0.06261	0.00047	396	7	392	3	391	3	0
9	0.36	0.05359	0.00113	0.48256	0.01227	0.06521	0.00085	354	29	400	8	407	5	-2
10	0.29	0.05530	0.00031	0.47779	0.00430	0.06265	0.00045	424	4	397	3	392	3	1
11	0.21	0.05584	0.00092	0.48703	0.01001	0.06339	0.00088	446	15	403	7	396	5	2
B10 (50°26'42.7"N, 87°36'23.3"E)														
1	0.34	0.05544	0.00034	0.52551	0.02017	0.06866	0.00175	430	9	429	12	428	12	0
2	0.14	0.05721	0.00026	0.57310	0.02644	0.07256	0.00209	500	8	460	12	452	12	2
3	0.04	0.05935	0.00038	0.46103	0.02181	0.05617	0.00210	580	12	385	12	352	8	9
4	0.21	0.05686	0.00028	0.53281	0.01744	0.06783	0.00192	486	11	434	16	423	16	3
5	0.33	0.05663	0.00030	0.59122	0.03156	0.07563	0.00184	477	9	472	16	470	16	0
6	0.25	0.05555	0.00026	0.52729	0.01924	0.06878	0.00181	434	8	430	12	429	12	0
7	0.12	0.05588	0.00032	0.53179	0.02325	0.06904	0.00155	448	9	433	12	430	16	1
8	0.24	0.06223	0.00341	0.47469	0.02307	0.05532	0.00204	682	120	394	72	347	12	12
9	0.37	0.06165	0.00060	0.90287	0.04694	0.10665	0.00580	662	52	653	25	653	34	0
10	0.34	0.06141	0.00053	0.76245	0.02402	0.09029	0.00296	654	32	575	14	557	18	-3
A24 (49°57'45.4"N, 88°04'30.2"E)														
1	0.33	0.05620	0.00049	0.53780	0.00723	0.06930	0.00067	460	14	437	5	432	4	1
2	0.23	0.05649	0.00046	0.53909	0.00730	0.06914	0.00068	472	14	438	5	431	4	2
3	0.43	0.05556	0.00035	0.52756	0.00552	0.06881	0.00056	435	11	430	4	429	3	0
4	0.58	0.05568	0.00047	0.51994	0.00600	0.06774	0.00055	440	13	425	4	422	3	1

TABLE 2
(continued)

Sample Spot No.	Ratios Th/U	$^{207}Pb/^{206}Pb$	1σ	$^{207}Pb/^{235}U$	1σ	$^{206}Pb/^{238}U$	1σ	Ages (Ma) $^{207}Pb/^{206}Pb$	1σ	$^{207}Pb/^{235}U$	1σ	$^{206}Pb/^{238}U$	1σ	Disc. (%)
A24 (49°57'45.4"N, 88°04'30.2"E)														
5	0.27	0.05633	0.00076	0.53381	0.01015	0.06883	0.00087	466	21	434	7	429	5	1
6	0.34	0.05895	0.00064	0.56553	0.00789	0.06963	0.00070	565	15	455	5	434	4	5
7	0.14	0.05610	0.00101	0.53022	0.01331	0.06880	0.00124	456	27	432	9	429	7	1
8	0.04	0.05662	0.00092	0.53932	0.01310	0.06893	0.00117	477	26	438	9	430	7	2
9	0.13	0.05425	0.00089	0.51673	0.01255	0.06884	0.00114	381	27	423	8	429	7	-1
10	0.37	0.05560	0.00047	0.53238	0.01303	0.06933	0.00158	436	24	433	9	432	10	0
11	0.12	0.05590	0.00039	0.52959	0.00611	0.06871	0.00063	448	12	432	4	428	4	1
12	0.65	0.05376	0.00061	0.50973	0.00774	0.06894	0.00076	361	16	418	5	430	5	-3
13	0.21	0.05515	0.00054	0.52446	0.00756	0.069	0.00071	418	16	428	5	430	4	0
14	0.27	0.06105	0.00054	0.78520	0.04529	0.09420	0.00526	641	56	588	26	580	31	-1
15	0.25	0.05869	0.00037	0.71937	0.02133	0.08908	0.00265	555	30	550	13	550	16	0
A01 (50°32'02.3"N, 88°10'32.0"E)														
1	0.33	0.05191	0.00263	0.29905	0.02017	0.04190	0.00175	282	90	266	20	265	15	0
2	0.23	0.05149	0.00236	0.27633	0.02190	0.03884	0.00209	263	90	248	20	246	15	1
3	0.43	0.05153	0.00301	0.29479	0.02644	0.04143	0.00209	264	90	262	15	262	10	0
4	0.58	0.06295	0.00262	0.34860	0.02097	0.04010	0.00184	707	75	304	15	253	10	17
5	0.27	0.06038	0.00234	0.30149	0.02106	0.03575	0.00205	617	180	268	30	226	10	16
6	0.34	0.05327	0.00510	0.24775	0.03156	0.03378	0.00184	340	40	225	10	214	5	5
7	0.25	0.06427	0.00247	0.34781	0.02141	0.03926	0.00199	750	40	303	10	248	10	18
8	0.04	0.05345	0.00235	0.27340	0.02772	0.03721	0.00272	348	45	245	10	236	10	4
9	0.13	0.05789	0.00217	0.29784	0.01887	0.03731	0.00200	526	520	265	55	236	10	11
10	0.37	0.05136	0.00248	0.28864	0.01924	0.04075	0.00181	257	50	257	10	257	10	0
11	0.34	0.05215	0.00315	0.28971	0.02571	0.04024	0.00202	292	70	258	15	254	10	2
12	0.24	0.05322	0.00272	0.29371	0.02260	0.04002	0.00201	338	40	261	10	253	5	3
13	0.36	0.05422	0.00281	0.30286	0.02307	0.04064	0.00204	380	60	269	15	257	15	4
14	0.21	0.05645	0.00283	0.30714	0.02430	0.03955	0.00215	470	55	272	15	250	15	8

Disc.(%) = $(1-(^{206}Pb/^{238}Pb)/(^{207}Pb/^{235}U))\times 100$.

TABLE 3

Zircon Lu-Hf isotopic compositions of granitoids in the Russian Altai

Spot No.	$^{176}Yb/^{177}Hf$	2σ	$^{176}Lu/^{177}Hf$	2σ	$^{176}Hf/^{177}Hf$	2σ	$t_{U\text{-}Pb}$	$(^{176}Hf/^{177}Hf)_i$	$\varepsilon_{Hf}(t)$	2σ	T_{DM}	2σ	T^{C}_{DM}	$f_{Lu/Hf}$
A30 (51°05'54.2"N, 85°35'8.7"E)														
1	0.073119	0.003200	0.002820	0.000109	0.282787	0.000037	401	0.282766	8.6	1.30	0.69	0.06	0.85	-0.92
2	0.054477	0.001190	0.002156	0.000041	0.282760	0.000032	401	0.282744	7.8	1.12	0.72	0.05	0.90	-0.94
3	0.045040	0.001470	0.001836	0.000061	0.282822	0.000023	401	0.282809	10.1	0.79	0.62	0.03	0.75	-0.94
4	0.038868	0.000103	0.001597	0.000003	0.282802	0.000038	401	0.282790	9.5	1.33	0.65	0.05	0.80	-0.95
5	0.049909	0.000842	0.002026	0.000032	0.282776	0.000038	401	0.282761	8.4	1.32	0.69	0.05	0.86	-0.94
6	0.093481	0.005890	0.003624	0.000223	0.282851	0.000047	401	0.282824	10.7	1.66	0.61	0.07	0.72	-0.89
7	0.057401	0.000663	0.002204	0.000025	0.282785	0.000041	401	0.282768	8.7	1.42	0.68	0.06	0.84	-0.93
8	0.054715	0.001185	0.002167	0.000046	0.282829	0.000037	401	0.282813	10.3	1.31	0.62	0.05	0.74	-0.93
9	0.041846	0.000544	0.001683	0.000017	0.282855	0.000035	401	0.282843	11.3	1.2	0.57	0.05	0.68	-0.95
A32 (51°05'54.2"N, 85°35'8.7"E)														
1	0.016668	0.000269	0.000805	0.000010	0.282817	0.000050	401	0.282811	10.2	1.76	0.61	0.07	0.75	-0.98
2	0.022617	0.000677	0.000994	0.000027	0.282871	0.000035	401	0.282863	12.1	1.22	0.54	0.05	0.63	-0.97
3	0.023204	0.000137	0.001084	0.000006	0.282810	0.000036	401	0.282802	9.9	1.26	0.63	0.05	0.77	-0.97
4	0.017302	0.000592	0.000799	0.000023	0.282750	0.000038	401	0.282744	7.8	1.34	0.71	0.05	0.90	-0.98
5	0.020016	0.000381	0.000905	0.000016	0.282773	0.000038	401	0.282766	8.6	1.32	0.68	0.05	0.85	-0.97
6	0.019472	0.000377	0.000836	0.000017	0.282869	0.000028	401	0.282863	12.0	0.99	0.54	0.04	0.63	-0.97
7	0.022563	0.000410	0.000976	0.000019	0.282865	0.000045	401	0.282858	11.9	1.56	0.55	0.06	0.64	-0.97
8	0.020728	0.000416	0.000882	0.000017	0.282782	0.000081	401	0.282775	8.9	2.83	0.67	0.11	0.83	-0.97
9	0.022593	0.000261	0.000974	0.000010	0.282755	0.000041	401	0.282748	8.0	1.44	0.70	0.06	0.89	-0.97
10	0.023503	0.000670	0.001052	0.000027	0.282833	0.000036	401	0.282825	10.7	1.25	0.60	0.05	0.72	-0.97
G4 (50°38'45.2"N, 86°18'44.8"E)														
1	0.028172	0.001199	0.001214	0.000040	0.282790	0.000045	370	0.282782	8.5	1.59	0.66	0.06	0.83	-0.96
2	0.025550	0.001200	0.001197	0.000055	0.282766	0.000039	370	0.282758	7.6	1.35	0.69	0.05	0.89	-0.96
3	0.037123	0.000658	0.001585	0.000031	0.282674	0.000045	370	0.282663	4.3	1.59	0.83	0.06	1.10	-0.95
4	0.017223	0.000411	0.000763	0.000018	0.282866	0.000056	370	0.282860	11.3	1.94	0.54	0.08	0.65	-0.98
5	0.019473	0.000170	0.000889	0.000008	0.282818	0.000036	370	0.282812	9.5	1.24	0.61	0.05	0.77	-0.97
6	0.018127	0.000218	0.000778	0.000009	0.282488	0.000099	370	0.282482	-2.1	3.45	1.08	0.14	1.51	-0.98

Table 3
(continued)

Spot No.	$^{176}Yb/^{177}Hf$	2σ	$^{176}Lu/^{177}Hf$	2σ	$^{176}Hf/^{177}Hf$	2σ	$t_{U\text{-}Pb}$	$(^{176}Hf/^{177}Hf)_i$	$\varepsilon_{Hf}(t)$	2σ	T_{DM}	2σ	T^{C}_{DM}	$f_{Lu/Hf}$
G4 (50°38'45.2"N, 86°18'44.8"E)														
7	0.021259	0.000891	0.000941	0.000037	0.282745	0.000093	370	0.282738	6.9	3.24	0.72	0.13	0.93	-0.97
8	0.025179	0.000324	0.001053	0.000015	0.282643	0.000039	370	0.282636	3.3	1.37	0.86	0.06	1.16	-0.97
9	0.022176	0.000962	0.000989	0.000047	0.282847	0.000049	370	0.282841	10.6	1.71	0.57	0.07	0.70	-0.97
10	0.027202	0.000204	0.001217	0.000010	0.282745	0.000046	370	0.282737	6.9	1.60	0.72	0.06	0.94	-0.96
11	0.021262	0.000277	0.000969	0.000015	0.282720	0.000037	370	0.282713	6.1	1.29	0.75	0.05	0.99	-0.97
12	0.033410	0.000632	0.001537	0.000025	0.282686	0.000058	370	0.282676	4.7	2.02	0.81	0.08	1.07	-0.95
13	0.019952	0.000333	0.000887	0.000015	0.282787	0.000029	370	0.282780	8.4	1.01	0.66	0.04	0.84	-0.97
14	0.024829	0.000067	0.001129	0.000003	0.282684	0.000043	360	0.282676	4.5	1.49	0.81	0.06	1.08	-0.97
A29 (50°38'42.8"N, 86°18'43.1"E)														
1	0.034246	0.000929	0.001496	0.000038	0.282713	0.000067	384	0.282702	6.0	2.36	0.77	0.10	1.01	-0.95
2	0.025640	0.000855	0.001198	0.000040	0.282774	0.000040	384	0.282765	8.2	1.41	0.68	0.06	0.86	-0.96
3	0.025073	0.000843	0.001097	0.000032	0.282729	0.000049	384	0.282722	6.7	1.71	0.74	0.07	0.96	-0.97
4	0.023950	0.001290	0.001119	0.000060	0.282599	0.000064	384	0.282591	2.0	2.24	0.93	0.09	1.26	-0.97
5	0.013697	0.000155	0.000659	0.000028	0.282489	0.000088	384	0.282485	-1.7	3.07	1.07	0.12	1.50	-0.98
6	0.030654	0.000963	0.001427	0.000057	0.282622	0.000091	384	0.282611	2.8	3.17	0.90	0.13	1.21	-0.96
7	0.024474	0.000553	0.001042	0.000024	0.282442	0.000081	384	0.282435	-3.5	2.82	1.15	0.11	1.61	-0.97
8	0.027135	0.001300	0.001255	0.000057	0.282530	0.000057	384	0.282521	-0.4	2.00	1.03	0.08	1.41	-0.96
9	0.020647	0.000556	0.000900	0.000021	0.282689	0.000077	384	0.282683	5.3	2.70	0.80	0.11	1.05	-0.97
11	0.023695	0.000688	0.001028	0.000026	0.282641	0.000084	384	0.282634	3.6	2.95	0.87	0.12	1.16	-0.97
12	0.019530	0.000594	0.000863	0.000031	0.282825	0.000090	384	0.282819	10.1	3.16	0.60	0.13	0.74	-0.97
13	0.028185	0.000303	0.001310	0.000016	0.282706	0.000057	384	0.282696	5.8	1.98	0.78	0.08	1.02	-0.96
14	0.059331	0.000903	0.002360	0.000034	0.282688	0.000040	384	0.282671	4.9	1.40	0.83	0.06	1.08	-0.93
A28 (50°37'49.1"N, 86°25'03.2"E)														
1	0.031649	0.001196	0.001507	0.000052	0.282638	0.000042	393	0.282627	3.5	1.48	0.88	0.06	1.17	-0.95
2	0.053809	0.004389	0.002390	0.000170	0.282677	0.000046	393	0.282659	4.7	1.61	0.85	0.07	1.10	-0.93
3	0.025167	0.000359	0.001182	0.000013	0.282643	0.000053	393	0.282634	3.8	1.87	0.87	0.08	1.15	-0.96
4	0.048262	0.002810	0.002164	0.000115	0.282536	0.000067	393	0.282519	-0.3	2.33	1.05	0.10	1.41	-0.93

Table 3
(continued)

Spot No.	$^{176}Yb/^{177}Hf$	2σ	$^{176}Lu/^{177}Hf$	2σ	$^{176}Hf/^{177}Hf$	2σ	$t_{U\text{-}Pb}$	$(^{176}Hf/^{177}Hf)_i$	$\varepsilon_{Hf}(t)$	2σ	T_{DM}	2σ	T^{C}_{DM}	$f_{Lu/Hf}$
A28 (50°37'49.1"N, 86°25'03.2"E)														
5	0.042526	0.003026	0.001904	0.000133	0.282418	0.000077	393	0.282403	-4.4	2.68	1.21	0.11	1.67	-0.94
6	0.047841	0.002640	0.002238	0.000121	0.282680	0.000029	393	0.282663	4.8	1.02	0.84	0.04	1.09	-0.93
7	0.040594	0.001047	0.001785	0.000040	0.282610	0.000034	393	0.282596	2.4	1.19	0.93	0.05	1.24	-0.95
8	0.043853	0.001081	0.002022	0.000043	0.282529	0.000068	393	0.282514	-0.5	2.38	1.05	0.10	1.42	-0.94
9	0.041502	0.000843	0.001879	0.000038	0.282695	0.000040	393	0.282680	5.4	1.39	0.81	0.06	1.05	-0.94
10	0.035230	0.001000	0.001637	0.000039	0.282667	0.000048	393	0.282654	4.5	1.69	0.84	0.07	1.11	-0.95
11	0.047939	0.004840	0.002341	0.000234	0.282524	0.000093	393	0.282507	-0.7	3.25	1.07	0.14	1.44	-0.93
12	0.045342	0.002982	0.002063	0.000124	0.282651	0.000049	393	0.282635	3.8	1.73	0.88	0.07	1.15	-0.94
A07 (50°06'18.1"N, 88°53'26.5"E)														
1	0.047465	0.000132	0.001844	0.000006	0.282905	0.000009	410	0.282891	13.2	0.32	0.50	0.01	0.56	-0.94
2	0.064543	0.000641	0.002429	0.000023	0.282763	0.000047	410	0.282745	8.0	1.63	0.72	0.07	0.89	-0.93
3	0.042664	0.000749	0.001676	0.000026	0.282750	0.000013	410	0.282737	7.8	0.46	0.72	0.02	0.91	-0.95
4	0.050157	0.002770	0.001951	0.000089	0.282741	0.000007	410	0.282726	7.4	0.24	0.74	0.01	0.93	-0.94
5	0.079546	0.001130	0.003022	0.000036	0.282677	0.000021	410	0.282654	4.8	0.73	0.86	0.03	1.10	-0.91
6	0.042917	0.001450	0.001647	0.000047	0.282672	0.000012	410	0.282659	5.0	0.41	0.84	0.02	1.09	-0.95
7	0.035313	0.000808	0.001393	0.000032	0.282763	0.000012	410	0.282752	8.3	0.42	0.70	0.02	0.88	-0.96
8	0.051718	0.001320	0.001971	0.000048	0.282601	0.000028	410	0.282586	2.4	0.99	0.95	0.04	1.25	-0.94
9	0.026741	0.000839	0.001196	0.000027	0.282778	0.000013	410	0.282768	8.9	0.45	0.68	0.02	0.84	-0.96
10	0.042908	0.000241	0.001640	0.000010	0.282722	0.000021	410	0.282710	6.8	0.73	0.76	0.03	0.97	-0.95
11	0.035364	0.000308	0.001410	0.000012	0.282748	0.000015	410	0.282737	7.8	0.52	0.72	0.02	0.91	-0.96
12	0.068724	0.001200	0.002589	0.000042	0.282814	0.000010	410	0.282794	9.8	0.34	0.65	0.01	0.78	-0.92
13	0.054528	0.000304	0.002072	0.000008	0.282803	0.000011	410	0.282787	9.6	0.37	0.66	0.02	0.80	-0.94
14	0.029892	0.000567	0.001179	0.000023	0.282640	0.000010	410	0.282631	4.0	0.36	0.87	0.01	1.15	-0.96
K03 (50°14'32"N, 87°58'49.2"E)														
1	0.018866	0.000232	0.000776	0.000009	0.282905	0.000018	394	0.282899	13.2	0.63	0.49	0.03	0.55	-0.98
2	0.030261	0.002045	0.001246	0.000079	0.282912	0.000018	394	0.282903	13.3	0.63	0.49	0.03	0.54	-0.96
3	0.021392	0.000459	0.000878	0.000017	0.282851	0.000017	394	0.282844	11.2	0.61	0.57	0.02	0.68	-0.97

Table 3
(continued)

Spot No.	$^{176}Yb/^{177}Hf$	2σ	$^{176}Lu/^{177}Hf$	2σ	$^{176}Hf/^{177}Hf$	2σ	$t_{U\text{-}Pb}$	$(^{176}Hf/^{177}Hf)_i$	$\varepsilon_{Hf}(t)$	2σ	T_{DM}	2σ	T^{C}_{DM}	$f_{Lu/Hf}$
K03 (50°14'32"N, 87°58'49.2"E)														
4	0.025948	0.000204	0.001035	0.000007	0.282821	0.000017	394	0.282814	10.1	0.59	0.61	0.02	0.75	-0.97
5	0.050588	0.000607	0.001965	0.000023	0.282867	0.000031	394	0.282852	11.5	1.08	0.56	0.04	0.66	-0.94
6	0.026743	0.000102	0.001075	0.000004	0.282839	0.000021	394	0.282831	10.7	0.75	0.59	0.03	0.71	-0.97
7	0.035533	0.000451	0.001417	0.000017	0.282928	0.000025	394	0.282918	13.8	0.89	0.46	0.04	0.51	-0.96
8	0.031224	0.000323	0.001256	0.000013	0.282851	0.000021	394	0.282842	11.1	0.74	0.57	0.03	0.68	-0.96
9	0.022215	0.000325	0.000964	0.000016	0.282778	0.000014	394	0.282771	8.6	0.50	0.67	0.02	0.84	-0.97
10	0.041737	0.000474	0.001640	0.000018	0.282848	0.000024	394	0.282836	10.9	0.84	0.58	0.03	0.69	-0.95
11	0.021997	0.000279	0.000895	0.000011	0.282902	0.000028	394	0.282896	13.0	0.97	0.49	0.04	0.56	-0.97
B10 (50°26'42.7"N, 87°36'23.3"E)														
1	0.019989	0.000591	0.000845	0.000025	0.282793	0.000040	445	0.282786	10.3	1.41	0.65	0.06	0.78	-0.97
2	0.051467	0.001550	0.002051	0.000061	0.282717	0.000036	445	0.282700	7.2	1.27	0.78	0.05	0.97	-0.94
3	0.044641	0.000632	0.001794	0.000023	0.282691	0.000040	445	0.282676	6.4	1.40	0.81	0.06	1.03	-0.95
4	0.036018	0.001975	0.001456	0.000074	0.282655	0.000073	445	0.282643	5.2	2.55	0.86	0.10	1.10	-0.96
5	0.044456	0.001550	0.001811	0.000064	0.282777	0.000040	445	0.282762	9.5	1.41	0.69	0.06	0.83	-0.95
6	0.036872	0.001160	0.001537	0.000044	0.282650	0.000058	445	0.282637	5.0	2.01	0.87	0.08	1.11	-0.95
7	0.046277	0.000872	0.001872	0.000033	0.282670	0.000046	445	0.282654	5.6	1.62	0.85	0.07	1.08	-0.94
8	0.029747	0.000171	0.001293	0.000007	0.282855	0.000023	445	0.282844	12.4	0.81	0.57	0.03	0.64	-0.96
A24 (49°57'45.4"N, 88°04'30.2"E)														
1	0.027244	0.000359	0.001341	0.000017	0.282903	0.000017	429	0.282892	13.7	0.58	0.50	0.02	0.55	-0.96
2	0.018146	0.001180	0.000899	0.000054	0.282817	0.000023	429	0.282810	10.8	0.81	0.62	0.03	0.73	-0.97
3	0.031634	0.002770	0.001475	0.000124	0.282758	0.000029	429	0.282747	8.5	1.02	0.71	0.04	0.88	-0.96
4	0.043074	0.002340	0.002050	0.000098	0.282855	0.000022	429	0.282838	11.8	0.77	0.58	0.03	0.67	-0.94
5	0.012576	0.000544	0.000610	0.000025	0.282889	0.000023	429	0.282884	13.4	0.79	0.51	0.03	0.56	-0.98
6	0.016590	0.000281	0.000811	0.000013	0.282878	0.000028	429	0.282871	13.0	0.96	0.53	0.04	0.59	-0.98
7	0.010423	0.000190	0.000530	0.000009	0.282773	0.000029	429	0.282769	9.3	1.01	0.67	0.04	0.83	-0.98
8	0.022564	0.000422	0.001116	0.000019	0.282837	0.000020	429	0.282828	11.4	0.71	0.59	0.03	0.69	-0.97
9	0.015349	0.000732	0.000798	0.000036	0.282830	0.000027	429	0.282824	11.3	0.94	0.60	0.04	0.70	-0.98

TABLE 3
(continued)

Spot No.	$^{176}Yb/^{177}Hf$	2σ	$^{176}Lu/^{177}Hf$	2σ	$^{176}Hf/^{177}Hf$	2σ	$t_{U\text{-}Pb}$	$\left(^{176}Hf/^{177}Hf\right)_i$	$\varepsilon_{Hf}(t)$	2σ	T_{DM}	2σ	T^{C}_{DM}	$f_{Lu/Hf}$
A24 (49°57'45.4"N, 88°04'30.2"E)														
10	0.022665	0.000481	0.001081	0.000020	0.282808	0.000021	429	0.282799	10.4	0.74	0.63	0.03	0.76	-0.97
11	0.055780	0.000117	0.002567	0.000005	0.282890	0.000022	429	0.282869	12.9	0.76	0.54	0.03	0.60	-0.92
12	0.045457	0.000620	0.002117	0.000027	0.282765	0.000030	429	0.282748	8.6	1.05	0.71	0.04	0.87	-0.94
13	0.042644	0.000877	0.001976	0.000038	0.282849	0.000023	429	0.282833	11.6	0.81	0.59	0.03	0.68	-0.94
A01 (50°32'02.3"N, 88°10'32.0"E)														
1	0.012204	0.000051	0.000552	0.000008	0.282799	0.000011	241	0.282797	6.2	0.37	0.63	0.01	0.88	-0.98
2	0.019037	0.000244	0.000797	0.000010	0.282696	0.000013	241	0.282692	2.5	0.46	0.78	0.02	1.12	-0.98
3	0.018025	0.000817	0.000776	0.000030	0.282837	0.000028	241	0.282834	7.5	0.98	0.59	0.04	0.80	-0.98
4	0.049188	0.002550	0.001916	0.000094	0.282682	0.000020	241	0.282674	1.8	0.71	0.83	0.03	1.16	-0.94
5	0.043227	0.004230	0.001732	0.000152	0.282737	0.000024	241	0.282729	3.8	0.84	0.74	0.03	1.03	-0.95
6	0.020839	0.000819	0.000909	0.000030	0.282702	0.000023	241	0.282698	2.7	0.79	0.78	0.03	1.11	-0.97
7	0.054097	0.001146	0.002202	0.000043	0.282719	0.000013	241	0.282709	3.0	0.45	0.78	0.02	1.08	-0.93
8	0.033605	0.000464	0.001468	0.000020	0.282776	0.000024	241	0.282770	5.2	0.83	0.68	0.03	0.94	-0.96
9	0.014594	0.000106	0.000704	0.000005	0.282768	0.000028	241	0.282765	5.0	0.98	0.68	0.04	0.95	-0.98
10	0.014181	0.000044	0.000741	0.000002	0.282786	0.000014	241	0.282782	5.7	0.50	0.66	0.02	0.91	-0.98
11	0.019932	0.000275	0.000875	0.000011	0.282782	0.000025	241	0.282778	5.5	0.88	0.66	0.04	0.92	-0.97
12	0.022281	0.001090	0.000990	0.000039	0.282772	0.000025	241	0.282767	5.1	0.88	0.68	0.04	0.95	-0.97
13	0.015500	0.000241	0.000722	0.000010	0.282763	0.000025	241	0.282760	4.9	0.89	0.69	0.04	0.97	-0.98
14	0.021239	0.000866	0.000924	0.000036	0.282680	0.000034	241	0.282676	1.9	1.20	0.81	0.05	1.15	-0.97

$\varepsilon_{Hf}(t)=10{,}000\times\{[(^{176}Hf/^{177}Hf)_S-(^{176}Lu/^{177}Hf)_S\times(e^{\lambda t}-1)]/[(^{176}Hf/^{177}Hf)_{CHUR,0}-(^{176}Lu/^{177}Hf)_{CHUR}\times(e^{\lambda t}-1)]-1\}$.

$T_{DM}=1/\lambda\times\ln\{1+[(^{176}Hf/^{177}Hf)_S-(^{176}Hf/^{177}Hf)_{DM}]/[(^{176}Lu/^{177}Hf)_S-(^{176}Lu/^{177}Hf)_{DM}]\}$.

$f_{Lu/Hf}=(^{176}Lu/^{177}Hf)_S/(^{176}Lu/^{177}Hf)_{CHUR}-1$.

$T^{c}_{DM}=t+1/\lambda\times\ln\{1+[(^{176}Hf/^{177}Hf)_{S,t}-(^{176}Hf/^{177}Hf)_{DM,t}]/[(^{176}Lu/^{177}Hf)_{LC}-(^{176}Lu/^{177}Hf)_{DM}]\}$.

where, $\lambda=1.867\times10{-}11$ year^{-1} (Soderlund and others, 2004); $(^{176}Lu/^{177}Hf)_S$ and $(^{176}Hf/^{177}Hf)_S$ are the measured values of the samples; $(^{176}Lu/^{177}Hf)_{CHUR}=0.0332$ and $(^{176}Hf/^{177}Hf)_{CHUR,0}=0.282772$ (Blichert-Toft and Albarède, 1997); $(^{176}Lu/^{177}Hf)_{DM}=0.0384$ and $(^{176}Hf/^{177}Hf)_{DM}=0.28325$ (Griffin and others, 2004); $(^{176}Lu/^{177}Hf)$lower crust$=0.019$; t=crystallization time of zircon.

Fig. 4. Cathodoluminescence images for representative zircons within granitoids in the Russian Altai. Solid and dashed circles indicate the locations of LA-ICPMS U-Pb dating and Hf analyses, respectively. The U-Pb age and $\varepsilon_{Hf}(t)$ values are given for each spot.

analyzed for U-Pb isotopic ratios and gave a quite broad range of $^{206}Pb/^{238}U$ age from 283 to 390 Ma, and an upper intercept age of 393 Ma (fig. 5E). The $\varepsilon_{Hf}(t)$ values of these zircons range from −4.4 to +5.4, and corresponding T^{C}_{DM} model ages are from 1.05 to 1.67 Ga (table 3 and fig. 6E).

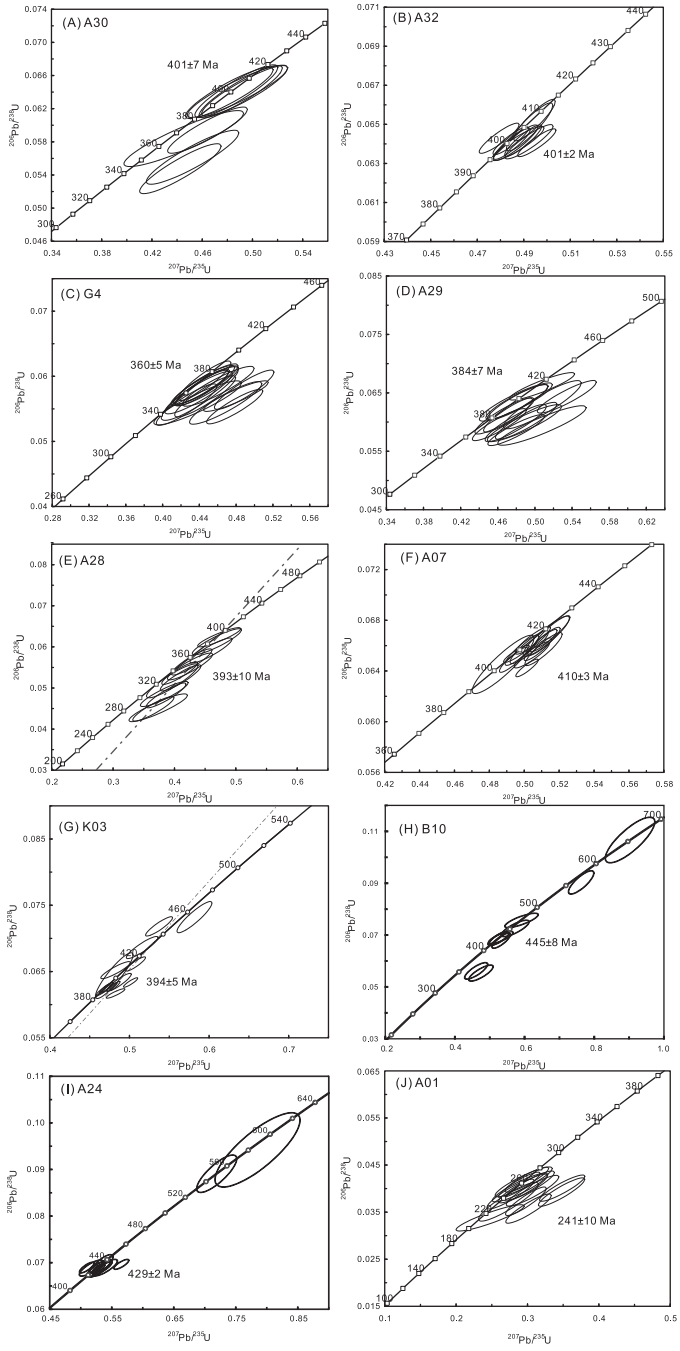

Fig. 5. Concordia diagrams showing zircon analyses from granitic rocks of the Russian Altai.

Granitic Samples of the Altai-Mongolian Terrane

Kokorya Pluton was emplaced into the Altai-Mongolian terrane and forms a dome with pseudo-tachylitic interlayer in the core. The outcrop area of the pluton is about 20

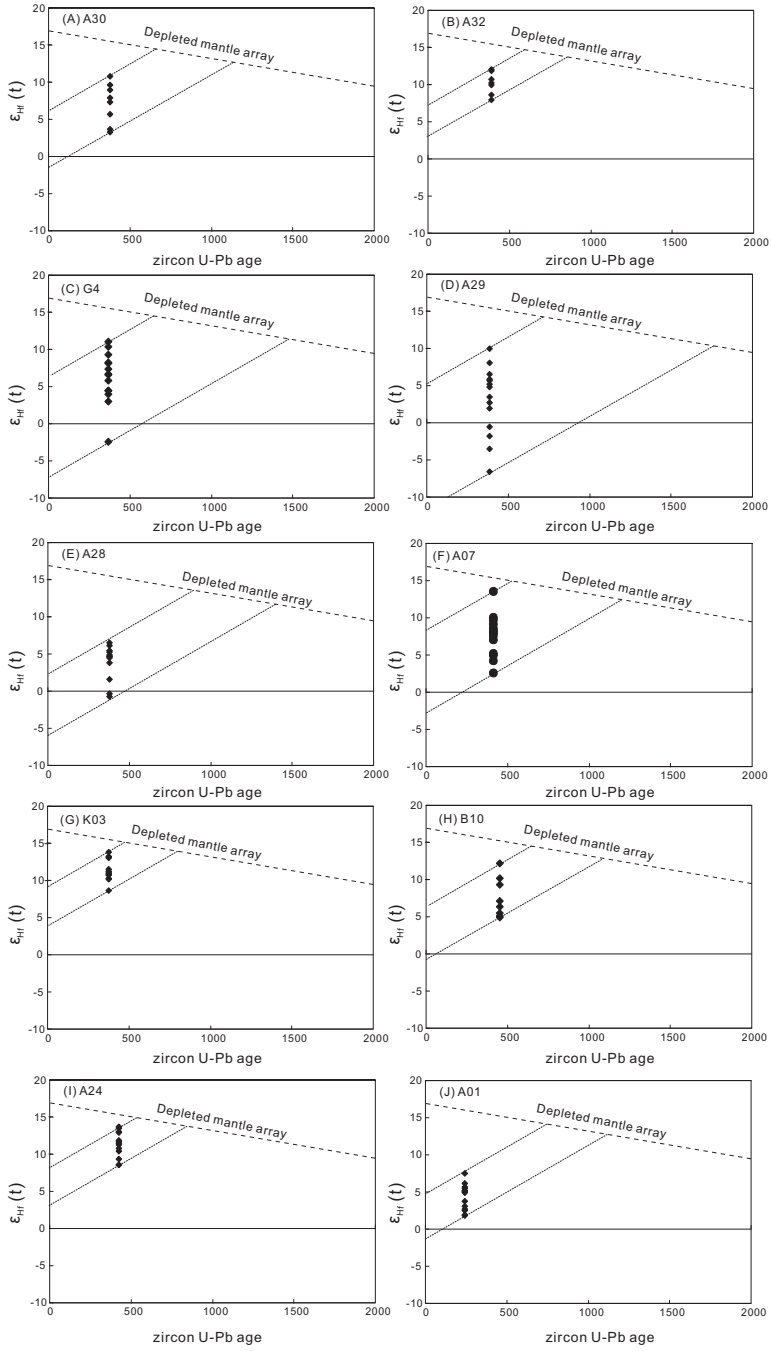

Fig. 6. Diagram of $\varepsilon_{Hf}(t)$ values versus zircon U-Pb ages of the Russian Altai granitic rocks.

km^2. In this region, terrigenous sediments, felsic tuffs and lavas thrust over metamorphic rocks of the Middle Paleozoic shear suture zone (figs. 2 and 3). A granite sample was collected from the pluton for zircon U-Pb dating and Hf isotopic analyses.

Sample A07: Zircons from this sample are characterized by euhedral and prismatic crystal shape, with oscillatory zoning and high Th/U ratios (table 2), indicating a magmatic origin. Fourteen zircon analyses of this sample yielded $^{206}Pb/^{238}U$ ages ranging from 401 to 419 Ma, with a weighted mean of 410 ±3 Ma (fig. 5F). The $\varepsilon_{Hf}(t)$ values of these zircons vary from +2.4 to +13.2, with T^{C}_{DM} model ages from 0.56 to 1.25 Ga (table 3 and fig. 6F).

Kurai granodiorite pluton is located to the northeast of the Kurai Village and intruded into a sequence of coal-bearing molasses in the Charysh-Terekta-Ulagan-Sayan suture-shear zone (CTUSs) (figs. 2 and 3). The granodiorite is dark gray in color and massive, with exposed area of less than 10 km^2 (fig. 3).

Sample K03: Zircons of this sample are characterized by euhedral and prismatic crystal shape, with oscillatory zoning in CL images and high Th/U ratios (table 2), suggesting magmatic origin. Eleven spot analyses give U-Pb ages ranging from 389 to 413 Ma, with a weighted mean $^{206}Pb/^{238}U$ age of 394 ±5 Ma (fig. 5G). The $\varepsilon_{Hf}(t)$ values of these zircons cluster between +8.6 to +13.8, with corresponding T^{C}_{DM} model ages ranging from0.51 to 0.84 Ga (table 3 and fig. 6G).

Granitic Samples of the CTUSs

Aktash North Batholith is situated in the Charysh-Terekta-Ulagan-Sayan suture-shear zone (CTUSs) (fig. 3). It intruded into the Early Paleozoic Teletsk accretionary complex. The exposed area of the batholith is about 50 km^2, and it consists mainly of coarse-grained two-mica granite and minor granodiorite. In this study, a rock of granite was collected for zircon U-Pb dating and Hf isotopic analyses.

Sample B10: Zircons from this sample have euhedral crystal shape and oscillatory zoning and high Th/U ratios, implying a magmatic origin. Two zircon analyses yield relatively older $^{206}Pb/^{238}U$ ages of 653 and 557 Ma (table 2), respectively, and the zircons are interpreted to be inherited. Other eight zircon analyses gave $^{206}Pb/^{238}U$ ages ranging from 347 to 470 Ma, and an upper intercept age of 445 Ma (fig. 5H). The $\varepsilon_{Hf}(t)$ values of these zircons vary from +5.0 to +12.4, and T^{C}_{DM} model ages are from 0.64 to 1.11 Ga (table 3 and fig. 6H).

Chagan-Uzun Pluton was emplaced into the Late Neoproterozoic primitive arc that is constituted of boninites, fore-arc turbidites and limestone. This pluton is small in size and consists mainly of granodiorite-diorite rocks. A massive granodiorite was sampled from the pluton for zircon U-Pb dating and Hf isotopic analyses.

Sample A24: Zircon CL images of this sample display euhedral and prismatic shape and oscillatory zoning (fig. 4), together with high Th/U ratios (>0.1), suggesting igneous origin. Two analyzed zircons yield relatively old $^{206}Pb/^{238}U$ ages of 580 and 550 Ma (table 2), respectively, and the zircons are considered to be inherited grains. Other thirteen zircon analyses give $^{206}Pb/^{238}U$ ages ranging from 422 to 434 Ma, and a weighted mean age of 429 ±2 Ma (table 2 and fig. 5I). The $\varepsilon_{Hf}(t)$ values of these zircons are from +8.5 to +13.7, with corresponding T^{C}_{DM} model ages from 0.55 to 0.88 Ga (table 3 and fig. 6I).

Ulagan Pluton occurs as a rounded intrusion and was emplaced into the Charysh-Terekta-Ulagan-Sayan suture-shear zone (CTUSs) (fig. 3). The country rocks consist mainly of turbidites, black shales, volcanic molasses, basalts. The exposed area of the pluton is about 80 km^2, and it consists mainly of coarse-grained massive two-mica granite. A representative sample was collected for zircon U-Pb dating and Hf isotopic analyses.

Sample A01: Zircons of this sample appear as euhedral, prismatic minerals, commonly with oscillatory zoning (fig. 4), which, together with high Th/U ratios, suggest an igneous origin. Fourteen zircon analyses yield $^{206}Pb/^{238}U$ ages ranging from 214 to 265 Ma and a weighted mean age of 241 ±10 Ma (table 2 and fig. 5J). The

$\varepsilon_{Hf}(t)$ values of these zircons vary from +1.8 to +7.5, and T^{C}_{DM} model ages are from 0.8 to 1.16 Ga (table 3 and fig. 6J).

DISCUSSIONS

Granitic Magmatism of the Russian Altai and Adjacent Regions

A great number of zircon U-Pb ages have been recently reported for tectonic blocks of the CAOB, and these data make it possible to constrain the timing of magmatism, tectonic evolution and basement nature (for example, Kröner and others, 2007; Sun and others, 2008, 2009; Jiang and others, 2012; Glorie and others, 2011; Rojas-Agramonate, 2011). For the Russian Altai, most of the granitic rocks were previously considered to be Devonian arc batholiths intruding into the Ediacaran-Cambrian accretionary complexes (Ota and others, 2007; Buslov and Safonova, 2010; Kruk and others, 2011), based on few reliable isotope geochronological data. Recently, Glorie and others (2011) have reported a series of zircon U-Pb data for igneous rocks and argued for multi-phase magmatic events associated with the geodynamic evolution from the Ediacaran-Cambrian to Late Paleozoic-Early Mesozoic.

Our zircon U-Pb dating results indicate that granitic magamtism of the region falls into three major episodes including 445~429 Ma, 410~360 Ma and ~241 Ma (table 2 and figs. 5A-5J). These age records are consistent with the proposed multi-phase magmatic events, which were probably related to several geodynamic scenarios including the Early Paleozoic composite Kazakhstan assembly (483-413 Ma), the Middle to Late Devonian collision between the Gorny Altai and Altai-Mongolian terrane (390-360 Ma) and the Late Carboniferous to Permian post-collisonal event (Glorie and others, 2011). Granitic intrusions from both the Gorny Altai terrane and the Altai-Mongolian terrane were emplaced in a similar time interval, although the two tectonic domains were previously suggested to have totally distinct tectonic affinities (Zonenshain and others, 1990; Mossakovsky and others, 1993; Ruzhentsev and Mossakovskiy, 1996; Dobretsov and others, 2003; Buslov and others, 2004a, 2004b; Dobretsov and Buslov, 2007; Glorie and others, 2011; Yang and others, 2011). The interesting finding above suggests that the two tectonic domains were possibly governed by the same geodynamic regime that was responsible for the intense granitic magmatism in the Devonian.

In the adjacent areas, early Paleozoic granites are also distributed in the Chinese Altai and Mongolian Altai, and most of them underwent high-grade metamorphism (Wang and others, 2006; Sun and others, 2008; Jiang and others, 2012). The Devonian granitiods represent a significant episode of magmatism in the Chinese Altai (Sun and others, 2009; Cai and others, 2011a, 2011b, 2011c), which is proposed to be associated with ridge subduction at the active margin of the Siberian continent (Sun and others, 2009; Wong and others, 2010; Cai and others, 2010, 2011a, 2011b, 2011c; Liu and others, 2012). The Mesozoic igneous rocks including A-type granitic plutons and numerous pegmatite dikes crop out widely in the Mongolian Altai and Chinese Altai (Wang and others, 2004, 2009; Zhu and others, 2006; Briggs and others, 2007; Jahn and others, 2009).

Possible Sources of the Granitic Magmas

The Ordovician-Silurian granitoids in the Russian Altai are low alkali and low alumina tonalite and trondhjemite, while the Devonian granitoids belong to peralkaline series and were named as A-type granitoids (Kruk and others, 2011). Based on tectonic setting and whole-rock Nd-Sr isotopic composition, Kruk and others (2011) proposed that the Ordovician-Silurian granitoids with positive $\varepsilon_{Nd}(t)$ values (+5.8 to +6.7) were most likely derived from partial melting of the basaltic rocks of Marianatype backarc basins, while the Devonian granitoids characterized by variable $\varepsilon_{Nd}(t)$

values (−2.0 to +4.4) probably originated from partial melting of basement rocks of turbidite basins. Similarly, almost all of our analyzed zircons yield positive $\varepsilon_{Hf}(t)$ values, which suggest that the magma sources were dominated by juvenile materials and ancient crustal materials are insignificant, as the case in the Chinese Altai (Sun and others, 2008; Cai and others, 2011a, 2011b, 2011c; Liu and others, 2012).

Several inherited zircons from samples B10 and A24 have Neoproterozoic ages (658-550 Ma, figs. 5H-5I and table 2), implying that the granitic magma source at lower and/or middle crustal level was possibly constituted of early stage igneous rocks in the region (Ota and others, 2007; Glorie and others, 2011). The zircon $\varepsilon_{Hf}(t)$ values of the Ordovician-Silurian granitoid rocks show a positive range from 5.0 to 13.7 (table 3 and figs. 6H-6I), and Hf crustal model ages (T^{C}_{DM}) of all these zircons range from 0.55 to 1.11 Ga (table 3), implying derivation from short-lived juvenile crustal source. Our data support the interpretation that the granitic magmas mainly resulted from melting of a juvenile source probably dominated by the Neoproterozoic to Early Paleozoic basaltic rocks formed widely in the intra-oceanic environments at early stage of the evolutionary history (Ota and others, 2007; Glorie and others, 2011).

In comparison, zircons in the Devonian granitoid rocks yield highly diverse $\varepsilon_{Hf}(t)$ values, although the majority of them have positive values (table 3 and figs. 6A-6G). It is noted that several zircons of the three samples (G4, A29 and A28) from the Gorny Altai terrane have negative $\varepsilon_{Hf}(t)$ values (table 3 and figs. 6C-6E), and their corresponding Hf model ages are from 1.61 Ga to 1.41 Ga, implying an involvement of reworking ancient continental crustal materials. However, it should be noted that zircons with positive $\varepsilon_{Hf}(t)$ values were predominant in the granitoid samples of the Gorny Altai terrane and, especially, the sample A32 is characterized by quite concentrated $\varepsilon_{Hf}(t)$ values ranging from 7.85 to 12.1 (table 3 and fig. 6B), which demonstrates that the Devonian granitoid rocks were produced dominantly by partial melting of juvenile materials. The two granitic intrusions with Devonian emplacement age from the Altai-Mongolian terrane have zircons all with positive $\varepsilon_{Hf}(t)$ values (table 3 and figs. 6F-6G), consistent with the interpretation that their parental magma was produced by partial melting of mainly short-lived juvenile materials. Similarly, variations in zircon Hf isotopic compositions of the granitoid rocks possibly reflect inhomogeneous characteristics of the source rocks, or mixing of juvenile materials with minor old crustal materials. This finding has been reported for the Chinese Altai where granitic rocks show wide spectrum of $\varepsilon_{Hf}(t)$ values ranging from 0 to +9 (Sun and others, 2008, 2009; Cai and others, 2011a).

The Early Triassic granitic intrusion, as a sticking pluton in the CTUSs, is characterized by abundant K-feldspar mineral assemblage and shows high alkali content, having affinity of post-collision A-type granite (Loiselle and Wones, 1979; Eby, 1992; Jahn and others, 2009; Shen and others, 2011). In the context of tectonic evolution of this area, the Triassic granitoids was suggested to be a product in an intra-plate environment. The pluton exhibits positive $\varepsilon_{Hf}(t)$ values ranging from 1.81 to 7.47 (table 3 and fig. 6J), and corresponding Hf model ages from 0.80 Ga to 1.16 Ga (table 3). These data together with evidence of petrology are consistent with the prevailed interpretation that the parental magma of A-type granite in the adjacent region was produced from enriched mantle-derived sources under an usually high temperature condition which is likely due to basaltic magma that underplated the lower crust (Debretsov, 2005; Jahn and others, 2009; Pirajno, 2010).

In summary, most of the granitoid rocks in the Russian Altai present comparable zircon Hf isotopic compositions, that is, the majority of zircons are characterized by positive $\varepsilon_{Hf}(t)$ values and Neoproterozoic crustal model ages, even though a few of them possess slightly negative $\varepsilon_{Hf}(t)$ values (−3.5 to −0.6) with older Hf model ages (table 3). It is inferred from zircon U-Pb and Hf isotope data that the juvenile crustal

materials produced in the early stage of the CAOB were probably dominant sources for later magmatism in the Russian Altai mountain range.

Continental Crustal Growth

It is commonly accepted that more than 50 percent of the crust within the CAOB is juvenile, and the CAOB thus represents the largest Phanerozoic crustal growth on the earth (Sengör and others, 1993; Sengör and Natal'in, 2004; Kovalenko and others, 1996, 2004; Jahn and others, 2000a, 2000b). Such a conclusion is largely based on the identification of numerous ophiolitic mélanges, island arcs and a large number of whole-rock Sm-Nd isotopic data (Kröner and others, 2013). However, it has been documented that quite a number of the ophiolitic complexes and arc rocks in the CAOB were generated in the Proterozoic, rather than the Phanerozoic (Khain and others, 2002; Rytsk and others, 2007). Moreover, increasing zircon U-Pb data reveal that numerous granitoid rocks in the CAOB with high positive whole-rock $\varepsilon_{Nd}(t)$ values were emplaced during a period of *ca.* 290 to 100 Ma, and these rocks were genetically associated with post-orogenic or intra-plate regimes (Han and others, 1997; Wang and others, 2004; Tong and others, 2007; Jahn and others, 2009), apparently posterior to the completion of accretionary processes of the CAOB. In this circumstance, a significant question with regard to the timing and mechanism of continental crust growth of the CAOB is still open to debate.

Experimental studies demonstrated that most granitoid magmas are partial melts of crustal materials at middle and/or lower crustal depth (Ebadi and Johannes, 1991; Rapp and others, 1991; Patiño Douce and Beard, 1995; Johannes and Holtz, 1996; Grochau and Johannes, 1997; Holtz and others, 2001; Tamic and others, 2001), although some granitoid plutons can originate directly from mantle-derived basaltic melts via significant fractional crystallization (Jagoutz and others, 2009; Jagoutz, 2010; Cai and others, 2012b). Thus, the ages of most granitoid rocks record timing of crustal melting events, not the real crustal residence times, whereas Nd or Hf isotope model ages may be used to assess timing of crustal rocks isolated from its depleted mantle source (DePaolo, 1981). Significant variations in $\varepsilon_{Hf}(t)$ value of zircons within granitoids usually represent magma mixing or heterogeneous source constituents. Mafic igneous rocks are rare relative to the widespread outcrops of granitoids in the Russian Altai mountain range. Additionally, there are few microgranular enclaves in the host granitoid intrusions, which suggest that magma mixing is not a significant process during granitoid mangmatism of the region. Therefore, zircon $\varepsilon_{Hf}(t)$ variations may indicate that their parental magmas were derived from heterogeneous source in the deep crust.

Zircon Hf model age is considered to represent an average crustal residence time, which can be applied to infer the history of crustal growth. In this study, granitoid rocks with Early Paleozoic emplacement ages show a variation in zircon Hf isotopic composition, with $\varepsilon_{Hf}(t)$ values ranging from -4.4 to $+13.8$ (table 3 and figs. 6A-6J), which corresponds to Hf model ages of 0.51 to 1.67 Ga, with three apparent peaks of 0.7 Ga, 0.9 Ga and 1.1 Ga (fig. 7). These model ages indicate that significant crustal growth events took place at several time intervals from the latest Mesoproterozoic to Early Paleozoic. A notable geological fact is that short-lived juvenile materials including ophiolites, seamount relics and arc assemblages of this age range occur in the northern CAOB (Kozakov and others, 1999; Khain and others, 2002; Rytsk and others, 2007; Demoux and others, 2009; Safonova and others, 2009; Utsunomiya and others, 2009), which allow us to consider that their counterparts may be buried at depth to constitute the lower and/or middle crust, while themselves exhumed on the surface may be as important provenances for the metasedimentary rocks in the region.

The above pieces of integrated evidence makes it possible to infer that several time intervals from the latest Mesoproterozoic to Early Paleozoic were likely of considerable

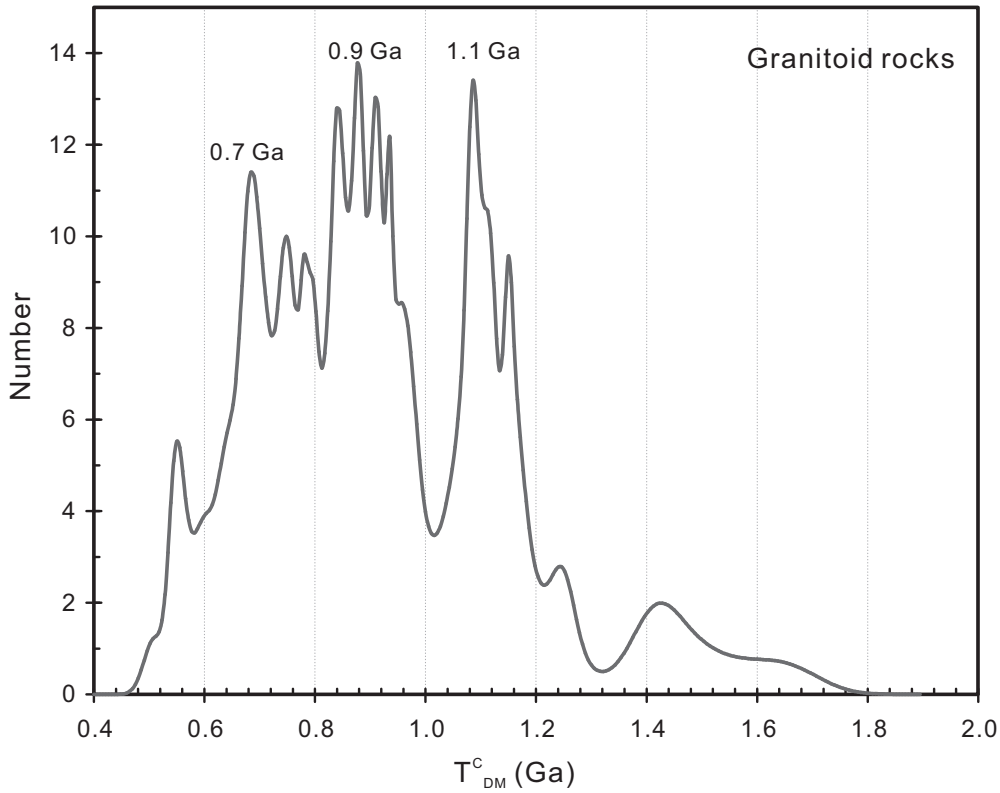

Fig. 7. Histogram for the distribution of Hf two-stage model ages (T^{C}_{DM}) of zircons from granitoids in the Russian Altai.

importance for continental crustal growth in the CAOB, and the Paleozoic granitoid rocks inherit the juvenile isotopic nature of the short-lived materials at depth. Consequently, massive Paleozoic granitic rocks maybe not represent continental crustal growth at the time when they were emplaced, but rather record reworking of relatively juvenile Proterozoic to Early Paleozoic rocks although mantle-derived mafic magma was possibly involved to serve as heat engine during granitic magma generation.

Implications for Tectonic Evolution

The geodynamic history of the immense CAOB has been controversially interpreted by competing models including a single arc model (Sengör and others, 1993; Sengör and Natal'in, 1996) and an archipelago model using the modern southwestern Pacific as an analogue (Dobertsov, 1995; Yakubchuk, 2004; Xiao and others, 2004, 2010; Windley and others, 2007; Wilhem and others, 2012). The latter is increasingly supported by several lines of geological evidence, that is, the CAOB contains diverse tectonic units with distinct nature and complicated amalgamation history (Windley and others, 2002, 2007; Kröner and others, 2007; Xiao and others, 2010). However, it has been documented that the arcs in the modern southwestern Pacific are mostly built on continental basement derived from the Australian continent (Smyth and others, 2007; Hall, 2011; Flores and others, 2011; Kröner and others, 2013), thus it is an important issue whether Precambrian continental blocks or basements are important components in the CAOB.

In the Russian Altai mountain range, the Gorny Altai terrane is considered as a tectonic collage of intra-oceanic island arcs and associated rocks, and it thus represents significant continental crustal growth through lateral accretion of oceanic blocks to Siberian continental margin at the early accretionary stage of the CAOB (Buslov and others, 2001, 2002; Dobretsov and others, 2004; Safonova and others, 2004, 2008, 2011; Ota and others, 2007; Utsunomiya and others, 2009; Glorie and others, 2011). The Gorny Altai and associated arc systems were accreted to Siberia or Peri-Siberian terranes by the Late Cambrian (Wilhem and others, 2012), and the Ordovician-Silurian granitoid rocks were generated by partial melting of these oceanic and arc rocks as a result of progressive subduction-accretion and collision.

In contrast, there is much debate on the geological nature of the Altai-Mongolian terrane. Some authors suggest that the Altai-Mongolian terrane was a microcontinent of Gondwanan origin (Zonenshain and others, 1990; Mossakovsky and others, 1993; Ruzhentsev and Mossakovskiy, 1996; Dobretsov and others, 2003; Buslov and others, 2004a, 2004b; Dobretsov and Buslov, 2007; Glorie and others, 2011; Yang and others, 2011), and was incorporated into the Siberian continent after the Early Ordovician (Wilhem and others, 2012). Accordingly, the Altai-Mongolian terrane was suggested to be a portion of Kazakhstan-Baikal composite continent (Dobretsov and Buslov, 2007), and finally amalgamated with Gorny Altai terrane during the Late Devonian to Early Carboniferous (Glorie and others, 2011). However, several lines of evidence do not support this interpretation. Firstly, the existence of the assumed ancient Precambrian basement is challenged by recent geochronological studies. For instance, the high-grade paragneissic rocks in the Chinese Altai and the western Mongolia were deposited in the Eary Paleozoic (Sun and others, 2008; Jiang and others, 2012), thus they cannot represent fragments of the ancient basements as previously thought (Li and others, 1996; Li and Poliyangsiji, 2001; and Buslov and Safonova, 2010). Secondly, this study shows that the Devonian granitoids rocks from the Gorny Altai have zircon Hf isotope compositions similar to their counterparts in the Chinese Altai (fig. 7), which may suggest that the two terranes have comparable magma sources. These findings imply that the Altai-Mongolian terrane is possibly similar to the Gorny Altai in tectonic nature and is strikingly distinct from ancient continents with Precambrian basements, such as Siberian, Tuva-Mongol massif, Tarim and North China Cratons (Rainbird and others, 1998; Khudoley and others, 2001; Zhao and others, 2005; Darby and Gehrels, 2006; Lu and others, 2006). Similar conclusion has been drawn based on the studies of sedimentary rocks and granitoids in the Chinese Altai (Long and others, 2007, 2010; Sun and others, 2008, 2009; Cai and others, 2011a, 2011b, 2011c, 2012a, 2012b; Jiang and others, 2011). Geochemical and geochronological studies indicate that the Altai-Mongolian terrane may represent an accretion-subduction complex located on the Neoproterozoic continental margin which, in turn, may be a Neoproterozoic arc system on the Tuva-Mongol block which drifted northwards as a small micro-continent from northern India of Gondwana supercontinent (Sun and others, 2008; Long and others, 2010; Jiang and others, 2011).

Extensive Devonian granitic magmatism was present in both the Gorny Altai and the Altai-Mongolian terranes, which suggests that the two main domains were probably under the same tectonic regime in that time. The process of accretion and collision along the Charysh-Terekta-Ulagan-Sayan suture-shear zone (CTUSs) is proposed to trigger the Devonian magmatism in the region (Ota and others, 2007; Glorie and others, 2011). The amalgamation process united the two blocks into a uniform Peri-Siberian tectonic domain, and an active continental margin was developed on the south side (in present-day coordinates). Numerous Early Paleozoic igneous rocks with arc affinity crop out along the south margin of the Altai-Mongolian terrane and indicate that this region had long been governed by ocean subduction regime at least

till Late Devonian (Windley and others, 2002; Wang and others, 2006; Niu and others, 2006; Yuan and others, 2007; Shan and others, 2007; Sun and others, 2008; Long and others, 2007, 2010; Wong and others, 2010; Cai and others, 2010, 2011a, 2011b, 2012a, 2012b). Therefore, current geological features do not support the formation of so-called Kazakhstan-Baikal composite continent before the amalgamation of the Gorny Altai with the Altai-Mongolian terrane in the Devonian. Recently, a ridge subduction model has been proposed to account for the Devonian tectono-thermal activities, such as intense magmatism, high-temperature metamorphism and isotopic features of the Chinese Altai (Windley and others, 2007; Sun and others, 2009; Cai and others, 2010, 2011a, 2011b, 2012b; Wong and others, 2010; Jiang and others, 2010; Shen and others, 2011; Liu and others, 2012). Whether the peculiar tectonic event influenced the Russian Altai mountain range needs to be verified.

CONCLUSIONS

Granitic magamtism of the Russian Altai mountain range mainly took place in three major episodes including 445~429 Ma, 410~360 Ma and ~241 Ma, corresponding to the proposed multi-phase geodynamic evolution of the region. The majority of zircons within the granitoids are characterized by dominantly positive $\varepsilon_{Hf}(t)$ values and Neoproterozoic crustal model ages, which suggests that these widespread oceanic and arc-related rocks produced in the early stage of CAOB probably acted as dominant sources for later magmatism in the Russian Altai mountain range. Zircon Hf model ages indicate that several time intervals from the latest Mesoproterozoic to Early Paleozoic were likely of considerable importance for continental crustal growth in the region, when accretionary history has already demonstrated to start. These findings support the interpretation that massive occurrence of granitic rocks may not represent continental crustal growth at the time when they were emplaced, but rather record reworking of relatively juvenile Proterozoic to Early Paleozoic primitive crustal rocks although mantle-derived mafic magma was possibly involved to serve as heat engine during granitic magma generation.

The Gorny Altai and Altai-Mongolian terranes possibly have similar tectonic natures, but were two independent accretionary systems before Devonian collision. The accretion and collision processes resulted in the Paleozoic granitoid magmatism and induced the two tectonic terranes to become a uniform tectonic domain as the Siberian continental margin in the facing ocean side till the oceanic basin was closed in the region.

ACKNOWLEDGMENTS

This study was financially supported by the Major Basic Research Project of the Ministry of Science and Technology of China (Grant: 2014CB448000), Hong Kong Research Grant Council (HKU705311P and HKU704712P), National Science Foundation of China (41273048, 41273012, 41230207, 41190070, 41190071 and 41190072.), the research grant of State Key Laboratory of Isotope Geochemistry, GIGCAS (SKLIG-KF-12-03), the Coucher Foundation for the joint Laboratory between HKU and GIGCAS, and the research project of the Institute of Geology and Mineralogy SB RAS. Drs. Hongyan Geng and Jean Wong are thanked for their laboratory assistance. The authors are very grateful to Dr. Tsutomu Ota and an anonymous reviewer for their critical reviews and constructive comments that significantly improved this manuscript. This work is a contribution to IGCP #592 Project "Continental construction in Central Asia," and this paper is dedicated to Professor Bor-ming Jahn for his great achievement in earth sciences.

References

Andersen, T., 2002, Correction of common lead in U–Pb analyses that do not report ^{204}Pb: Chemical Geology, v. 192, n. 1–2, p. 59–79, http://dx.doi.org/10.1016/S0009-2541(02)00195-X

Belousova, E. A., Griffin, W. L., and O'Reilly, S. Y., 2006, Zircon crystal morphology, trace element signatures and Hf-isotope composition as a tool for petrogenetic modelling: examples from eastern Australian granitoids: Journal of Petrology, v. 47, n. 2, p. 329–353, http://dx.doi.org/10.1093/petrology/egi077

Berzin, N. A., and Dobretsov, N. L., 1994, Geodynamic evolution of southern Siberia in late Precambrian-early Palaeozoic time, *in* Coleman, R. G., editor, Reconstruction of the Paleo-Asian Ocean: Utrecht, The Netherlands, Proceedings of the 29th International Geological Congress, Part B, VSP, p. 53–70.

Black, L. P., Kamo, S. L., Allen, C. M., Aleinikoff, J. N., Davis, D. W., Korsch, R. J., and Foudoulis, C., 2003, TEMORA 1: a new zircon standard for Phanerozoic U–Pb geochronology: Chemical Geology, v. 200, n. 1–2, p. 155–170, http://dx.doi.org/10.1016/S0009-2541(03)00165-7

Blichert-Toft, J., and Albarède, F., 1997, The Lu–Hf geochemistry of the chondrites and the evolution of the mantle–crust system: Earth and Planetary Science Letters, v. 148, n. 1–2, p. 243–258, http://dx.doi.org/10.1016/S0012-821X(97)00040-X

Blichert-Toft, J., Chauvel, C., and Albarède, F., 1997, Separation of Hf and Lu for high-precision sotope analysis of rock samples by magnetic sector-multiple collector ICP-MS: Contributions to Mineralogy and Petrology, v. 127, n. 3, p. 248–260, http://dx.doi.org/10.1007/s004100050278

Briggs, S. M., Yin, A., Manning, C. E., Chen, Z.-L., Wang, X.-F., and Grove, M., 2007, Late Paleozoic tectonic history of the Ertix Fault in the Chinese Altai and its implications for the development of the Central Asian Orogenic System: Geological Society of America Bulletin, v. 119, n. 7–8, p. 944–960, http://dx.doi.org/10.1130/B26044.1

Buslov, M. M., 2011, Tectonics and geodynamics of the Central Asian Foldbelt: the role of Late-Palaeozoic large-amplitude displacements: Russian Geology and Geophysics, v. 52, n. 1, p. 52–71, http://dx.doi.org/10.1016/j.rgg.2010.12.005

Buslov, M. M., and Safonova, I. Y., 2010, Guide-book for the Post-symposium Excursion of Siberian continent margins, Altai-Mongolian Gondwana-derived terrane and their separating suture-shear zone: Novosibirsk, Russia, 74 p.

Buslov, M. M., and Watanabe, T., 1996, Intrasubduction collision and its role in the evolution of an accretionary wedge: the Kurai zone of Gorny Altai, Central Asia: Russian Geology and Geophysics, v. 36. p. 83–94.

Buslov, M. M., Berzin, N. A., Dobretsov, N. L., and Simonov, V. A., 1993, Geology and tectonics of Gorny Altai, *in* Dobretsov, N. L., editor, Guide-book for the Post-symposium Excursion of the 4th International Symposium of the IGCP project 283: "Geodynamic Evolution of the Paleoasian Ocean": Novosibirsk, Russia, 122 p.

Buslov, M. M., Safonova, I. Y., and Bobrov, V. A., 1998, New geochemical data on boninites from Kurai ophiolites, Gorny Altai: Doklady Earth Sciences, v. 361, p. 244–247.

Buslov, M. M., Safonova, I. Y., Watanabe, N., Obut, O. T., Fujiwara, I., Iwata, K., Semakov, N. N., Sugai, Y., Smirnova, L. V., and Kazanskii, A. Y., 2001, Evolution of the Palaeo-Asian Ocean (Altai-Sayan Region, Central Asia) and collision of possible Gondwana-derived terranes with the southern marginal part of the Siberian continent: Geosciences Journal, v. 5, n. 1, p. 203–204, http://dx.doi.org/10.1007/BF02910304

Buslov, M. M., Watanabe, T., Saphonova, I. Y., Iwata, K., Travin, A., and Akiyama, M., 2002, A Vendian–Cambrian island arc system of the Siberian continent in Gorny Altai (Russia, Central Asia): Gondwana Research, v. 5, n. 4, p. 781–800, http://dx.doi.org/10.1016/S1342-937X(05)70913-8

Buslov, M. M., Fujiwara, Y., Iwata, K., and Semakov, N. N., 2004a, Late Paleozoic-Early Mesozoic geodynamics of Central Asia: Gondwana Research, v. 7, n. 3, p. 791–808, http://dx.doi.org/10.1016/S1342-937X(05)71064-9

Buslov, M. M., Watanabe, T., Fujiwara, Y., Iwata, K., Smirnova, L. V., Safonova, I. Y., Semakov, N. N., and Kiryanova, A. P., 2004b, Late Paleozoic faults of the Altai region, Central Asia: tectonic pattern and model of formation: Journal of Asian Earth Sciences, v. 23, n. 5, p. 655–671, http://dx.doi.org/10.1016/S1367-9120(03)00131-7

Cai, K. D., Sun, M., Yuan, C., Zhao, G. C., Xiao, W. J., Long, X. P., and Wu, F. Y., 2010, Geochronological and geochemical study of mafic dykes from the northwest Chinese Altai: Implications for petrogenesis and tectonic evolution: Gondwana Research, v. 18, n. 4, p. 638–652, http://dx.doi.org/10.1016/j.gr.2010.02.010

——— 2011a, Prolonged magmatism, juvenile nature and tectonic evolution of the Chinese Altai, NW China: Evidence from zircon U-Pb and Hf isotopic study of Paleozoic granitoids: Journal of Asian Earth Sciences, v. 42, n. 5, p. 949–968, http://dx.doi.org/10.1016/j.jseaes.2010.11.020

——— 2011b, Geochronology, petrogenesis and tectonic significance of peraluminous granites from the Chinese Altai, NW China: Lithos, v. 127, n. 1–2, p. 261–281, http://dx.doi.org/10.1016/j.lithos.2011.09.001

Cai, K. D., Sun, M., Yuan, C., Long, X. P., and and Xiao, W. J., 2011c, Geological framework and Paleozoic tectonic history of the Chinese Altai, NW China: a review: Russian Geology and Geophysics, v. 52, n. 12, p. 1619–1633, http://dx.doi.org/10.1016/j.rgg.2011.11.014

Cai, K. D., Sun, M., Yuan, C., Zhao, G. C., Xiao, W. J., and Long, X. P., 2012a, Keketuohai mafic-ultramafic complex in the Chinese Altai, NW China: petrogenesis and geodynamic significance: Chemical Geology, v. 294–295, p. 26–41, http://dx.doi.org/10.1016/j.chemgeo.2011.11.031

Cai, K. D., Sun, M., Yuan, C., Xiao, W. J., Zhao, G. C., Long, X. P., and Wu, F. Y., 2012b, Carboniferous mantle-derived felsic intrusion in the Chieese Altai, NW China: implications for geodynamic change of

the accretionary orogenic belt: Gondwana Research, v. 22, n. 2, p. 681–698, http://dx.doi.org/10.1016/j.gr.2011.11.008
Darby, B. J., and Gehrels, G., 2006, Detrital zircon reference for the North China block: Journal of Asian Earth Sciences, v. 26, n. 6, p. 637–648, http://dx.doi.org/10.1016/j.jseaes.2004.12.005
Demoux, A., Kroner, A., Liu, D. Y., and Badarch, G., 2009, Precambrian crystalline basement in southern Mongolia as revealed by SHRIMP zircon dating: International Journal of Earth Sciences, v. 98, n. 6, p. 1365–1380, http://dx.doi.org/10.1007/s00531-008-0321-4
DePaolo, D. J., 1981, Trace element and isotopic effects of combined wallrock assimilation and fractional crystallization: Earth and Planetary Science Letters, v. 53, n. 2, p. 189–202, http://dx.doi.org/10.1016/0012-821X(81)90153-9
Dobretsov, N. L., 2005, 250 Ma large igneous provinces of Asia: Siberian and Emeishan traps (plateau basalts) and associated granitoids: Russian Geology and Geophysics, v. 46, n. 9, p. 870–890.
Dobretsov, N. L., and Buslov, M. M., 2007, Late Cambrian-Ordovician tectonics and geodynamics of the Central Aisa: Russian Geology and Geophysics, v. 48, n. 1, p. 71–82, http://dx.doi.org/10.1016/j.rgg.2006.12.006
Dobretsov, N. L., Buslov, M. M., and Vernikovsky, V. A., 2003, Neoproterozoic to Early Ordovician evolution of the Paleo-Asian Ocean: implications to the break-up of Rodinia: Gondwana Research, v. 6, n. 2, p. 143–159, http://dx.doi.org/10.1016/S1342-937X(05)70966-7
Dobretsov, N. L., Buslov, M. M., and Yu, U. C., 2004, Fragments of oceanic islands in accretion-collision areas of Gorny Altai and Salair, southern Siberia, Russia: early stages of continental crustal growth of the Siberian continent in Vendian-Early Cambrian time: Journal of Asian Earth Sciences, v. 23, n. 5, p. 673–690, http://dx.doi.org/10.1016/S1367-9120(03)00132-9
Ebadi, A., and Johannes, W., 1991, Beginning of melting and composition of first melts in the system Qz-Ab-Or-H_2O-CO_2: Contributions to Mineralogy and Petrology, v. 106, n. 3, p. 286–295, http://dx.doi.org/10.1007/BF00324558
Eby, G. N., 1992, Chemical subdivision of the A-type granitoids: petrogenetic and tectonic implications: Geology, v. 20, n. 7, p. 641–644, http://dx.doi.org/10.1130/0091-7613(1992)020⟨0641:CSOTAT⟩2.3.CO;2
Flores, J. A., Spencer, C. J., Harris, R. A., and Hoiland, C., 2011, Provenance of Permian-Triassic Gondwana sequence units accreted to the Banda Arc: Constraints from U/Pb and Hf analysis of zircons and igneous geochemistry: San Francisco, American Geophysical Union, v. 51, abstract #T51A-2303, p. F2303.
Glorie, S., De Grave, J., Buslov, M. M., Zhimulev, F. I., Izmer, A., Vandoorne, W., Ryabinin, A., Van den haute, P., Vanhaecke, F., and Elburg, M. A., 2011, Formation and Palaeozoic evolution of the Gorny-Altai–Altai-Mongolia suture zone (South Siberia): Zircon U/Pb constraints on the igneous record: Gondwana Research, v. 20, n. 2–3, p. 465–484, http://dx.doi.org/10.1016/j.gr.2011.03.003
Griffin, W. L., Belousova, E. A., Shee, S. R., Pearson, N. J., and O'Reilly, S. Y., 2004, Archean crustal evolution in the northern Yilgarn Craton: U–Pb and Hf-isotope evidence from detrital zircons: Precambrian Research, v. 131, n. 3–4, p. 231–282, http://dx.doi.org/10.1016/j.precamres.2003.12.011
Grochau, B., and Johannes, W., 1997, Stability of phlogopite in granitic melts, as experimental investigation: Contributions to Mineralogy and Petrology, v. 126, n. 3, p. 315–330, http://dx.doi.org/10.1007/s004100050253
Hall, R. M., 2011, Australia-SE Asia collision: plate tectonics and crustal flow, *in* Hall, R., Cottam, M. A., and Wilson, M. E. J., editors, The SE Asian gateway: history and tectonics of Australia-Asia collision: Geological Society, London, Special Publications, v. 355, p. 75–109, http://dx.doi.org/10.1144/SP355.5
Han, B. F., Wang, S. G., Jahn, B. M., Hong, D. W., Kagami, H., and Sun, Y. L., 1997, Depleted-mantle source for the Ulungur River A-type granites from North Xinjiang, China: geochemistry and Nd–Sr isotopic evidence, and implications for Phanerozoic crustal growth: Chemical Geology, v. 138, n. 3–4, p. 135–159, http://dx.doi.org/10.1016/S0009-2541(97)00003-X
Holtz, F., Johannes, W., Tamic, N., and Behrens, H., 2001, Maximum and minimum water contents of granitic melts generated in the crust: a reevaluation and implications: Lithos, v. 56, n. 1, p. 1–14, http://dx.doi.org/10.1016/S0024-4937(00)00056-6
Hong, D., Wang, S., Xie, X., and Zhang, J., 2001, The Phanerozoic continental growth in Central Asia and the evolution of Laurasia supercontinent: Gondwana Research, v. 4, n. 4, p. 632–633, http://dx.doi.org/10.1016/S1342-937X(05)70435-4
Hoskin, P. W. O., and Schaltegger, U., 2003, The composition of zircon and igneous and metamorphic petrogenesis: Reviews in Mineralogy and Geochemistry, v. 53, n. 1, p. 27–62, http://dx.doi.org/10.2113/0530027
Jagoutz, O. E., 2010, Construction of the granitoid crust of an island arc. Part II: a quantitative petrogenetic model: Contributions to Mineralogy and Petrology, v. 160, n. 3, p. 359–381, http://dx.doi.org/10.1007/s00410-009-0482-6
Jagoutz, O. E., Burg, J. P., Hussain, S., Dawood, H., Pettke, T., Iizuka, T., and Maruyama, S., 2009, Construction of the granitoid crust of an island arc part I: geochronological and geochemical constraints from the plutonic Kohistan (NW Pakistan): Contributions to Mineralogy and Petrology, v. 158, n. 6, p. 739–755, http://dx.doi.org/10.1007/s00410-009-0408-3
Jahn, B. M., Wu, F. Y., and Chen, B., 2000a, Massive granitoid generation in Central Asia: Nd isotope evidence and implication for continental growth in the Phanerozoic: Episodes, v. 23, p. 82–92.
Jahn, B. M., Wu, F., and Chen, B., 2000b, Granitoids of the Central Asian orogenic belt and continental growth in the Phanerozoic: Transaction of Royal Society of Edinburgh-Earth Science, v. 91, n. 1–2, p. 181–193, http://dx.doi.org/10.1017/S0263593300007367
Jahn, B. M., Capdevila, R., Liu, D. Y., Vernon, A., and Badarch, G., 2004, Sources of Phanerozoic granitoids in the transect Bayanhongor-Ulaan Baatar, Mongolia: geochemical and Nd isotopic evidence, and

implications for Phanerozoic crustal growth: Journal of Asian Earth Sciences, v. 23, n. 5, p. 629–653, http://dx.doi.org/10.1016/S1367-9120(03)00125-1

Jahn, B. M., Litvinovsky, B. A., Zanvilevich, A. N., and Reichow, M., 2009, Peralkaline granitoid magmatism in the Mongolian-Transbaikalian Belt: Evolution, petrogenesis and tectonic significance: Lithos, v. 113, n. 3–4, p. 521–539, http://dx.doi.org/10.1016/j.lithos.2009.06.015

Jiang, Y. D., Sun, M., Zhao, G. C., Yuan, C., Xiao, W. J., Xia, X. P., Long, X. P., and Wu, F. Y., 2010, The ~390 Ma high-T metamorphism in the Chinese Altai: A consequence of ridge-subduction?: American Journal of Science, v. 310, p, 1421–1452, http://dx.doi.org/10.2475/10.2010.08

——— 2011, Precambrian detrital zircons in the Early Paleozoic Chinese Altai: Their provenance and implications for the crustal growth of central Asia: Precambrian Research, v. 189, n. 1–2, p. 140–154, http://dx.doi.org/10.1016/j.precamres.2011.05.008

Jiang, Y. D., Sun, M., Kröner, A., Tumurkhuu, D., Long, X. P., Zhao, G. C., Yuan, C., and Xiao, W. J., 2012, The high-grade Tseel Terrane in SW Mongolia: An Early Paleozoic arc system or a Precambrian sliver?: Lithos, v. 142–143, p. 95–115, http://dx.doi.org/10.1016/j.lithos.2012.02.016

Johannes, W., and Holtz, F., 1996, Petrogenesis and Experimental Petrology of Granitic Rocks: Berlin, Springer, 335 p.

Khain, E. V., Bibokova, E. V., Kroner, A., Zhuravlev, D. Z., Sklyarov, E. V., Fedotova, A. A., and Kravchenko-Berezhnoy, I. R., 2002, The most ancient ophiolites of the Central Asian fold belt: U-Pb and Pb-Pb zircon ages for the Dunzhugur complex, Eastern Sayan, Siberia, and geodynamic implications: Earth and Planetary Science Letters, v. 199, n. 3–4, p. 311–325, http://dx.doi.org/10.1016/S0012-821X(02)00587-3

Khudoley, A. K., Rainbird, R. H., Stern, R. A., Kropachev, A. P., Heaman, L. M., Zanin, A. M., Podkovyrov, V. N., Belova, V. N., and Sukhorukov, V. I., 2001, Sedimentary evolution of the Riphean-Vendian basin of southeastern Siberia: Precambrian Research, v. 111, n. 1–4, p. 129–163, http://dx.doi.org/10.1016/S0301-9268(01)00159-0

Kovalenko, V. I., Yarmolyuk, V. V., Kovach, V. P., Kotov, A. B., Kozakov, I. K., and Sal'nikova, E. B., 1996, Sources of Phanerozoic granitoids in Central Asia: Sm-Nd isotope data: Geochemistry International, v. 34, n. 8, p. 628–640.

Kovalenko, V. I., Yarmolyuk, V. V., Kovach, V. P., Kotov, A. B., Kozakov, I. K., Sal'nikova, E. B., and Larin, A. M., 2004, Isotope provinces, mechanisms of generation and sources of the continental crust in the Central Asian Mobile Belt: geological and isotopic evidence: Journal of Asian Earth Sciences, v. 23, n. 5, p. 605–627, http://dx.doi.org/10.1016/S1367-9120(03)00130-5

Kozakov, I. K., Kotov, A. B., Sal'nikova, E. B., Bibikova, E. V., Kovach, V. P., Kirnozova, T. I., Berezhnaya, N. G., and Lykhin, D. A., 1999, Metamorphic age of crystalline complexes of the Tuva–Mongolia Massif: the U–Pb geochronology of granitoids: Petrology, v. 7, p. 177–191.

Kröner, A., Windley, B. F., Badarch, G., Tomurtogoo, O., Hegner, E., Jahn, B. M., Gruschka, S., Khain, E. V., Demoux, A., and Wingate, M. T. D., 2007, Accretionary growth and crust formation in the Central Asian Orogenic Belt and comparison with the Arabian–Nubian shield: Geological Society of America Memoirs, v. 200, p. 181–209, http://dx.doi.org/10.1130/2007.1200(11)

Kröner, A., Kovach, V., Belousova, E., Hegner, E., Armstrong, R., Dolgopolova, A., Seltmann, R., Alexeiev, D. V., Hoffmann, J. E., Wong, J., Sun, M., Cai, K. D., Wang, T., Tong, Y., Wilde, S. A., Degtyarev, K. E., and Rytsk, E., 2013, Reassessment of continental growth during the accretionary history of the Central Asian Orogenic Belt: Gondwana Research, http://dx.doi.org/10.1016/j.gr.2012.12.023

Kruk, N. N., Rudnev, S. N., Vladimirov, A. G., Shokalsky, S. P., Kovach, V. P., Serov, P. A., and Volkova, N. I., 2011, Early-Middle Paleozoic granitoids in Gorny Altai, Russia: Implications for continental crust history and magma sources: Journal of Asian Earth Sciences, v. 42, n. 5, p. 928–948, http://dx.doi.org/10.1016/j.jseaes.2010.12.008

Kuzmichev, A., Kröner A., Hegner, E., Liu, D. Y., and Wan, Y. S., 2005, The Shishkhid ophiolite, northern Mongolia: A key to the reconstruction of a Neoproterozoic island–arc system in central Asia: Precambrian Research, v. 138, n. 1–2, p. 125–150, http://dx.doi.org/10.1016/j.precamres.2005.04.002

Li, H. J., He, G. Q., Wu, T. R., and Wu, B., 2006, Confirmation of Altai-Mongolia microcontinent and its implications: Acta Petrologica Sinica, v. 22, p. 1369–1379 (in Chinese).

Li, T. D., and Poliyangsiji, B. H., 2001, Tectonics and crustal evolution of Altai in China and Kazakhstan: Xinjiang Geology, v. 19, p. 27–32 (in Chinese with English abstract).

Li, T. D., Qi, Z. M., Xiao, S. L., and Wu, B. Q., 1996, New improvement of comparative study of geology and mineralization of Altai between China and Kazakhstan, in Thesis Volume of the Symposium of the 8th Five Year Plan of Geoscience for Contribution to 30th IGC: Beijing, Chinese Geological Society, Metallurgical Industrial Publishing House, p. 256–259 (in Chinese).

Litvinovsky, B. A., Tsygankova, A. A., Jahn, B. M., Katzir, Y., and Be'eri-Shlevin, Y., 2011, Origin and evolution of overlapping calc-alkaline and alkaline magmas: The Late Palaeozoic post-collisional igneous province of Transbaikalia (Russia): Lithos, v. 125, n. 3–4, p. 845–874, http://dx.doi.org/10.1016/j.lithos.2011.04.007

Liu, W., Liu, X. J., and Xiao, W. J., 2012, Massive granitoid production without massive continental-crust growth in the Chinese Altay: Insight into the source rock of granitoids using integrated zircon U-Pb age, Hf-Nd-Sr isotopes and geochemistry: American Journal of Science, v. 312, n. 6, p. 629–684, http://dx.doi.org/10.2475/06.2012.02

Liu, Y., Hu, Z., Gao, S., Günther, D., Xu, J., Gao, C., and Chen, H., 2008, *In situ* analysis of major and trace elements of anhydrous minerals by LA–ICP-MS without applying an internal standard: Chemical Geology, v. 257, n. 1–2, p. 34–43, http://dx.doi.org/10.1016/j.chemgeo.2008.08.004

Loiselle, M. C., and Wones, D. R., 1979, Characteristics and origin of anorogenic granites: Geological Society of America Abstracts with Programs, v. 11, p. F468.

Long, X. P., Sun, M., Yuan, C., Xiao, W. J., Lin, S. F., Wu, F. Y., Xia, X. P, and Cai, K. D., 2007, Detrital zircon age and Hf isotopic studies for metasedimentary rocks from the Chinese Altai: Implications for the Early

Paleozoic tectonic evolution of the Central Asian Orogenic Belt: Tectonics, v. 26, n. 5, TC5015, 20 p., http://dx.doi.org/10.1029/2007TC002128

Long, X. P., Yuan, C., Sun, M., Xiao, W. J., Zhao, G. C., Wang, Y. J., and Cai, K. D., 2010, Detrital zircon ages and Hf isotopes of the early Paleozoic Flysch sequence in the Chinese Altai, NW China: New constraints on depositional age, provenance and tectonic evolution: Tectonophysics, v. 480, n. 1–4, p. 213–231, http://dx.doi.org/10.1016/j.tecto.2009.10.013

Lu, X. P., Wu, F. Y., Guo, J. H., Wilde, S. A., Yang, J. H., Liu, X. M., and Zhang, X. O., 2006, Zircon U–Pb geochronological constraints on the Paleoproterozoic crustal evolution of the Eastern block in the North China Craton: Precambrian Research, v. 146, n. 3–4, p. 138–164, http://dx.doi.org/10.1016/j.precamres.2006.01.009

Ludwig, K. R., 2003, User's Manual for Isoplot 3.00: A Geochronological Toolkit for Microsoft Excel: Berkeley, Berkeley Geochronology Center, Special Publication N. 4a, 70 p.

Mossakovsky, A. A., Ruzhentsev, S. V., Samygin, S. G., and Kheraskova, T. N., 1993, Central Asian fold belt: geodynamic evolution and history of formation: Geotektonika, v. 26, p. 455–473 (in Russia).

Niu, H. C., Sato, H., Zhang, H. X., Jun'ichi Ito, Yu, X. Y., Nagao, T., Terada, K., and Zhang, Q., 2006, Juxtaposition of adakite, boninite, high-TiO2 and low-TiO2 basalts in the Devonian southern Altay, Xinjiang, NW China: Journal of Asian Earth Sciences, v. 28, n. 4–6, p. 439–456, http://dx.doi.org/10.1016/j.jseaes.2005.11.010

Ota, T., Utsunomiya, A., Uchio, Y., Isozaki, Y., Buslov, M. M., Ishikawa, A., Maruyama, S., Kitajima, K., Kaneko, Y., Yamamoto, H., and Katayama, I., 2007, Geology of the Gorny Altai subduction–accretion complex, southern Siberia: Tectonic evolution of an Ediacaran–Cambrian intra-oceanic arc-trench system: Journal of Asian Earth Sciences, v. 30, n. 5–6, p. 666–695, http://dx.doi.org/10.1016/j.jseaes.2007.03.001

Patiño Douce, A. E., and Beard, J. S., 1995, Dehydration-melting of biotite gneiss and quartz amphibolite from 3 to 15 kbar: Journal of Petrology, v. 36, n. 3, p. 707–738, http://dx.doi.org/10.1093/petrology/36.3.707

Pirajno, F., 2010, Intracontinental strike-slip faults, associated magmatism, mineral systems and mantle dynamics: examples from NW China and Altay-Sayan (Siberia): Journal of Geodynamics, v. 50, n. 3–4, p. 325–346, http://dx.doi.org/10.1016/j.jog.2010.01.018

Rainbird, R. H., Stern, R. A., Khudoley, A. K., Kropachev, A. P., Heaman, L. M., and Sukhorukov, V. I., 1998, U-Pb geochronology of Riphean sandstone and gabbro from southeast Siberia and its bearing on the Laurentia-Siberia connection: Earth and Planetary Science Letters, v. 164, n. 3–4, p. 409–420, http://dx.doi.org/10.1016/S0012-821X(98)00222-2

Rapp, B. R., Watson, E. B., and Miller, C. F., 1991, Partial melting of amphibolite/eclogite and the origin of Archean trondhjemites and tonalities: Precambrian Research, v. 51, n. 1–4, p. 1–25, http://dx.doi.org/10.1016/0301-9268(91)90092-O

Reichow, M. K., Litvinovsky, B. A., Parrish, R. R., and Saunders, A. D., 2010, Multi-stage emplacement of alkaline and peralkaline syenite-granite suites in the Mongolian-Transbaikalian Belt, Russia: Evidence from U-Pb geochronology and whole rock geochemistry: Chemical Geology, v. 273, n. 1–2, p. 120–135, http://dx.doi.org/10.1016/j.chemgeo.2010.02.017

Rojas-Agramonte, Y., Kröner, A., Demoux, A., Xia, X. P., Wang, W., Donskaya, T., Liu, D. Y., and Sun, M., 2011, Detrital and xenocrystic zircon ages from Neoproterozoic to Palaeozoic arc terranes of Mongolia: significance for the origin of crustal fragments in the Central Asian Orogenic Belt: Gondwana Research, v. 19, n. 3, p. 751–763, http://dx.doi.org/10.1016/j.gr.2010.10.004

Rudnev, S. N., Vladimirov, A. G., Ponomarchuk, V. A., Kruk, N. N., Babin, G. A., and Borisov, S. M., 2004, Early Paleozoic granitoid batholiths of the Altai-Sayan folded region (lateral-temporal zoning and sources): Doklady Earth Sciences, v. 396, n. 3, p. 492–495 (In Russian).

Rudnev, S. N., Borisov, S. M., Babin, G. A., Levchenkov, O. A., Makeev, A. F., Serov, P. A., Matukov, D. I., and Plotkina, Y. V., 2008, Early Paleozoic batholiths in the northern part of the Kuznetsk Alatau: composition, age, and sources: Petrology, v. 16, n. 4, p. 395–419, http://dx.doi.org/10.1134/S086959110804005X

Ruzhentsev, S. V., and Mossakovskiy, A. A., 1996, Geodynamics and tectonic evolution of the Central Asian Paleozoic structures as the result of the interaction between the Pacific and Indo-Atlantic segments of the Earth: Geotectonics, v. 29, p. 294–311.

Rytsk, E. Yu., Kovach, V. P., Yarmolyuk, V. V., and Kovalenko, V. I., 2007, Structure and evolution of the continental crust in the Baikal Fold Region: Geotectonics, v. 41, n. 6, p. 440–464, http://dx.doi.org/10.1134/S0016852107060027

Safonova, I. Yu., Buslov, M. M., Iwata, K., and Kokh, D. A., 2004, Fragments of Vendian–early Carboniferous oceanic crust of the Paleo-Asian Ocean in foldbelts of the Altai-Sayan region of Central Asia: geochemistry, biostratigraphy and structural setting: Gondwana Research, v. 7, n. 3, p. 771–790, http://dx.doi.org/10.1016/S1342-937X(05)71063-7

Safonova, I. Y., Simonov, V. A., Buslov, M. M., Ota, T., and Maruyama, S., 2008, Neoproterozoic basalts of the Paleo-Asian Ocean (Kurai accretionary zone, Gorny Altai, Russia): geochemistry, petrogenesis, and geodynamics: Russian Geology and Geophysics, v. 49, n. 4, p. 254–271, http://dx.doi.org/10.1016/j.rgg.2007.09.011

Safonova, I. Yu., Utsunomiya, A., Kojima, S., Nakae, S., Tomurtogoo, O., Filippov, A. N., and Koizumi, K., 2009, Pacific superplume-related oceanic basalts hosted by accretionary complexes of Central Asia, Russian Far East and Japan: Gondwana Research, v. 16, n. 3–4, p. 587–608, http://dx.doi.org/10.1016/j.gr.2009.02.008

Safonova, I. Y., Buslov, M. M., Simonov, V. A., Izokh, A. E., Komiya, T., Kurganskaya, E. V., and Ohno, T., 2011, Geochemistry, petrogenesis and geodynamic origin of basalts from the Katun' accretionary complex of Gorny Altai (southwestern Siberia): Russian Geology and Geophysics, v. 52, n. 4, p. 421–442, http://dx.doi.org/10.1016/j.rgg.2011.03.005

Scherer, E., Münker, C., and Mezger, K., 2001, Calibration of the lutetium–hafnium clock: Science, v. 293, n. 5530, p. 683–687, http://dx.doi.org/10.1126/science.1061372

Şengör, A. M. C., and Natal'in, B. A., 1996, Paleotectonics of Asia: fragments of a synthesis, *in* Yin, A., and Harrison, M., editors, The tectonic evolution of Asia: Cambridge, Cambridge University Press, p. 486–640.

——— 2004, Phanerozoic analogues of Archaean oceanic basement fragments: Altaid ophiolites and ophirags, *in* Kusky, T. M., editor, Precambrian Ophiolites and Related Rocks: Amsterdam, Elsevier, Developments in Precambrian Geology, v. 13, p. 675–726, http://dx.doi.org/10.1016/S0166-2635(04)13021-1

Şengör, A. M. C., Natal'in, B. A., and Burtman, V. S., 1993, Evolution of the Altaid tectonic collage and Paleozoic crustal growth in Eurasia: Nature, v. 364, p. 299–307, http://dx.doi.org/10.1038/364299a0

Shan, Q., Niu, H. C., Yu, X. Y., and Zeng, Q. S., 2007, Geochemical characteristics, magmatic genesis and tectonic background of the late Paleozoic high potassium and high silicon ignimbrite on the southern margin of Altaid, north Xinjiang: Acta Petrologica Sinica, v. 23, p. 1721–1729 (in Chinese with English abstract).

Shen, X. M., Zhang, H. X., Wang, Q., Wyman, D. A., and Yang, Y. H., 2011, Late Devonian-Early Permian A-type granites in the southern Altay Range, Northwest China: Petrogenesis and implications for tectonic setting of "A_2-type" granites: Journal of Asian Earth Science, v. 42, n. 4, p. 986–1007, http://dx.doi.org/10.1016/j.jseaes.2010.10.004

Smyth, H. R., Hamilton, P. L., Hall, R., and Kinny, P. D., 2007, The deep crust beneath island arcs: Inherited zircons reveal a Gondwana continental fragment beneath East Java, Indonesia: Earth and Planetary Science Letters, v. 258, n. 1–2, p. 269–282, http://dx.doi.org/10.1016/j.epsl.2007.03.044

Sun, M., Yuan, C., Xiao, W., Long, X., Xia, X., Zhao, G., Lin, S., Wu, F., and Kröner, A., 2008, Zircon U–Pb and Hf isotopic study of gneissic rocks from the Chinese Altai: progressive accretionary history in the early to middle Paleozoic: Chemical Geology, v. 247, n. 3–4, p. 352–383, http://dx.doi.org/10.1016/j.chemgeo.2007.10.026

Sun, M., Long, X. P., Cai, K. D., Jiang, Y. D., Wang, B. Y., Yuan, C., Zhao, G. C., Xiao, W. J., and Wu, F. Y., 2009, Early Paleozoic ridge subduction in the Chinese Altai: insight from the abrupt change in Zircon Hf isotopic compositions: Science in China, Series D, v. 52, n. 9, p. 1345–1358, http://dx.doi.org/10.1007/s11430-009-0110-3

Tamic, N., Behrens, H., and Holtz, F., 2001, The solubility of H_2O and CO_2 in rhyolitic melts in equilibrium with a mixed CO_2-H_2O fluid phase: Chemical Geology, v. 174, n. 1–3, p. 333–347, http://dx.doi.org/10.1016/S0009-2541(00)00324-7

Tong, Y., Wang, T., Hong, D. W., Dai, Y. J., Han, B. F., and Liu, X. M., 2007, Ages and origin of the early Devonian granites from the north part of Chinese Altai Mountains and its tectonic implications: Acta Petrologica Sinica, v. 23, n. 8, p. 1933–1944.

Tsygankova, A. A., Litvinovsky, B. A., Jahn, B. M., Reichow, M. K., Liu, D. Y., Larionov, A. N., Presnyakovf, S. L., Lepekhina, Ye. N., and Sergeev, S. A., 2010, Sequence of magmatic events in the Late Paleozoic of Transbaikalia, Russia (U-Pb isotope data): Russian Geology and Geophysics, v. 51, n. 9, p. 972–994, http://dx.doi.org/10.1016/j.rgg.2010.08.007

Utsunomiya, A., Jahn, B., Ota, T., and Safonova, I. Y., 2009, A geochemical and Sr–Nd isotopic study of the Vendian greenstones from Gorny Altai, southern Siberia: implications for the tectonic setting of the formation of greenstones and the role of oceanic plateaus in accretionary orogen: Lithos, v. 113, n. 3–4, p. 437–453, http://dx.doi.org/10.1016/j.lithos.2009.05.020

Vladimirov, A. G., Kozlov, M. S., Shokal'skii, S. P., Khalilov, V. A., Rudnev, S. N., Kruk, N. N., Vystavnoi, S. A., Borisov, S. M., Berezikov, Y. K., Metsner, A. N., Babin, G. A., Mamlin, A. N., Murzin, O. M., Nazarov, G. V., and Makarov, V. A., 2001, Major epochs of intrusive magmatism of Kuznetsk Alatau, Altai, and Kalba (from U–Pb isotope dates): Russian Geology and Geophysics, v. 42, n. 8, p. 1157–1178.

Volkova, N. I., and Sklyarov, E. V., 2007, High-pressure complexes of Central Asian Fold Belt: geologic setting, geochemistry, and geodynamic implications: Russian Geology and Geophysics, v. 48, n. 1, p. 83–90, http://dx.doi.org/10.1016/j.rgg.2006.12.008

Volkova, N. I., Stupakov, S. I., Tret'yakov, G. A., Simonov, V. A., Travin, A. V., and Yudin, D. S., 2005, Blueschists from the Uimon Zone as evidence for Ordovician accretionarycollisional events in Gorny Altai: Russian Geology and Geophysics, v. 46, p. 361–378.

Wang, T., Zheng, Y. D., Li, T. B., and Gao, Y. J., 2004, Mesozoic granitic magmatism in extensional tectonics near the Mongolian border in China and its implications for crustal growth: Journal of Asian Earth Sciences, v. 23, n. 5, p. 715–729, http://dx.doi.org/10.1016/S1367-9120(03)00133-0

Wang, T., Hong, D. W., Jahn, B. M., Tong, Y., Wang, Y. B., Han, B. F., and Wang, X. X., 2006, Timing, petrogenesis, and setting of Palaeozoic synorogenic intrusions from the Altai Mountains, Northwest China: implications for the tectonic evolution of an accretionary orogen: The Journal of Geology, v. 114, n. 6, p. 735–751, http://dx.doi.org/10.1086/507617

Wang, T., Jahn, B. M., Kovach, V. P., Tong, Y., Hong, D. W., and Han, B. F., 2009, Nd-Sr isotopic mapping of the Chinese Altai and implications for continental growth in the Central Asian Orogenic Belt: Lithos, v. 110, n. 1–4, p. 359–372, http://dx.doi.org/10.1016/j.lithos.2009.02.001

Wilhem, C., Windley, B. F., and Stampfli, G. M., 2012, The Altaids of Central Asia: A tectonic and evolutionary innovative review: Earth-Science Reviews, v. 113, n. 3–4, p. 303–341, http://dx.doi.org/10.1016/j.earscirev.2012.04.001

Windley, B. F., Kröner, A., Guo, J., Qu, G., Li, Y., and Zhang, C., 2002, Neoproterozoic to Palaeozoic geology of the Altai orogen, NW China: New zircon age data and tectonic evolution: Journal of Geology, v. 110, n. 6, p. 719–739, http://dx.doi.org/10.1086/342866

Windley, B. F., Alexeiev, D., Xiao, W., Kroner, A., and Badarch, G., 2007, Tectonic models for accretion of

the Central Asian Orogenic Belt: Journal of the Geological Society, London, v. 164, n. 1, p. 31–47, http://dx.doi.org/10.1144/0016-76492006-022

Wong, K., Sun, M., Zhao, G. C., Yuan, C., and Xiao, W. J., 2010, Geochemical and geochronological studies of the Alegedayi Ophiolitic Complex and its implication for the evolution of the Chinese Altai: Gondwana Research, v. 18, n. 23, p. 438–454, http://dx.doi.org/10.1016/j.gr.2010.01.010

Xia, X. P., Sun, M., Geng, H., Sun, Y., Wang, Y., and Zhao, G. C., 2011, Quasi-simultaneous determination of U–Pb and Hf isotope compositions of zircon by excimer laser-ablation multiple-collector ICPMS: Journal of Analytical Atomic Spectrometry, v. 26, n. 9, p. 1868–1871, http://dx.doi.org/10.1039/c1ja10116a

Xiao, W. J., Windley, B. F., Badararch, G., Sun, S., Li J., Qin, K., and Wang, Z., 2004, Palaeozoic accretionary and convergent tectonics of the southern Altaids: implications for the growth of central Asia: Journal of the Geological Society, London, v. 161, p. 339–342, http://dx.doi.org/10.1144/0016-764903-165

Xiao, W. J., Han, C. M., Yuan, C., Sun, M., Lin, S. F., Chen, H. L., Li, Z. L., Li, J. L., and Sun, S., 2008, Middle Cambrian to Permian subduction-related accretionary orogenesis of Northern Xinjiang, NW China: Implications for the tectonic evolution of Central Asia: Journal of Asian Earth Sciences, v. 32, n. 2–3, p. 102–117, http://dx.doi.org/10.1016/j.jseaes.2007.10.008

Xiao, W. J., Windley, B. F., Yuan, C., Sun, M., Han, C. M., Lin, S. F., Chen, H. L., Yan, Q. R., Liu, D. Y., Qin, K. Z., Li, J. L., and Sun, S., 2009, Paleozoic multiple subduction-accretion processes of the southern Altaids: American Journal of Science, v. 309, n. 3, p. 221–270, http://dx.doi.org/10.2475/03.2009.02

Xiao, W. J., Huang, B. C., Han, C. M., Sun, S., and Li, J. L., 2010, A review of the western part of the Altaids: A key to understanding the architecture of accretionary orogens: Gondwana Research, v. 18, n. 2–3, p. 253–273, http://dx.doi.org/10.1016/j.gr.2010.01.007

Yakubchuk, A., 2004, Architecture and mineral deposit settings of the Altaid orogenic collage: a revised model: Journal of Asian Earth Sciences, v. 23, n. 5, p. 761–779, http://dx.doi.org/10.1016/j.jseaes.2004.01.006

Yang, T. N., Li, J. Y., Zhang, J., and Hou, K. J., 2011, The Altai-Mongolia terrane in the Central Asian Orogenic Belt (CAOB): A peri-Gondwana one? Evidence from zircon U-Pb, Hf isotopes and REE abundances: Precambrian Research, v. 187, n. 1–2, p. 79–98, http://dx.doi.org/10.1016/j.precamres.2011.02.005

Yuan, C., Sun, M., Xiao, W. J., Li, X. H., Chen, H. L., Lin, S. F., Xia, X. P., and Long, X. P., 2007, Accretionary orogenesis of the Chinese Altai: Insights from Paleozoic granitoids: Chemical Geology, v. 242, n. 1–2, p. 22–39, http://dx.doi.org/10.1016/j.chemgeo.2007.02.013

Zhao, G. C., Sun, M., Wilde, S. A., and Li, S. Z., 2005, Late Archean to Paleoproterozoic evolution of the North China Craton: Key issues revisited: Precambrian Research, v. 136, n. 2, p. 177–202, http://dx.doi.org/10.1016/j.precamres.2004.10.002

Zhu, Y. F., Zeng, Y. S., and Gu, L. B., 2006, Geochemistry of the rare metal-bearing pegmatite No. 3 vein and related granites in the Keketuohai region, Altay Mountains, northwest China: Journal of Asian Earth Sciences, v. 27, n. 1, p. 61–77, http://dx.doi.org/10.1016/j.jseaes.2005.01.007

Zonenshain, L. P., Kuzmin, M. I., Natapov, L. M., and Page, B. M., 1990, Geology of the USSR: a plate tectonic synthesis: American Geophysical Union, Geodynamics Series Monograph, v. 21, p. F242, http://dx.doi.org/10.1029/GD021